AD-A106 380 NAVAL OCEAN SYSTEMS CENTER SAN DIEGO CA F/G 17/2.1
SKYWAVE COMMUNICATION TECHNIQUES. DECISION FEEDBACK EQUALIZATIO--ETC(U)
MAR 81 L E HOFF, A R KING
UNCLASSIFIED NOSC/TR-709 NL

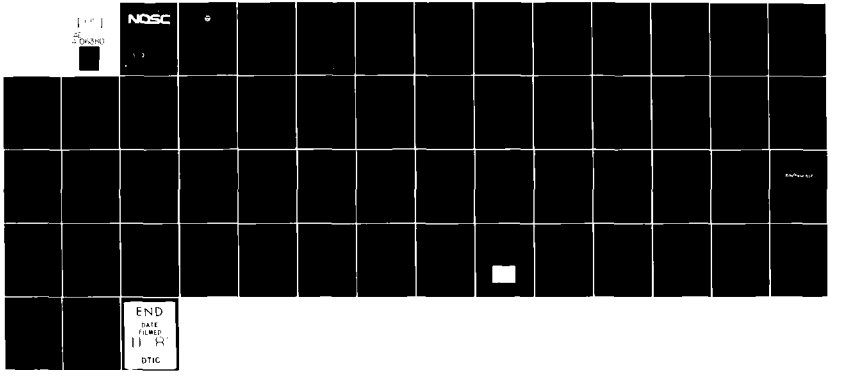

(12) LEVEL II

NOSC

NOSC TR 709

NOSC TR 709

Technical Report 709

SKYWAVE COMMUNICATION TECHNIQUES

Decision feedback equalization for serially modulated spread-spectrum signals in the hf band yields improved reliability

LE Hoff
AR King

30 March 1981

Project Final Report for Period FY77 - FY81

Prepared for
Naval Electronic Systems Command
Code PME 110-21

Approved for public release; distribution unlimited

NAVAL OCEAN SYSTEMS CENTER
SAN DIEGO, CALIFORNIA 92152

NAVAL OCEAN SYSTEMS CENTER, SAN DIEGO, CA 92152

AN ACTIVITY OF THE NAVAL MATERIAL COMMAND

SL GUILLE, CAPT, USN
Commander

HL BLOOD
Technical Director

ADMINISTRATIVE INFORMATION

Work was performed under Program Element 24163N, Project X0695-CC (NOSC 814-CM14) by members of the Rf and Acoustic Communications Technology Branch (Code 8112) for Naval Electronic Systems Command, Code PME 110-21. This report covers work from FY77 through FY81.

Released by
MS Kvigne, Head
Communications Research
and Technology Division

Under authority of
HD Smith, Head
Communications Systems and
Technology Department

METRIC CONVERSION

To convert from	to	Multiply by
statute miles	km	~ 1.61
nautical miles	km	~ 1.85
feet	m	~ 3.05×10^{-1}

UNCLASSIFIED

SECURITY CLASSIFICATION OF THIS PAGE *(When Data Entered)*

REPORT DOCUMENTATION PAGE

READ INSTRUCTIONS BEFORE COMPLETING FORM

1. REPORT NUMBER: NOSC Technical Report 709 (TR 709)	2. GOVT ACCESSION NO.: AD-A106 380
3. RECIPIENT'S CATALOG NUMBER:	
4. TITLE *(and Subtitle)*: SKYWAVE COMMUNICATION TECHNIQUES, Decision feedback equalization for serially modulated spread-spectrum signals in the hf band yields improved reliability	5. TYPE OF REPORT & PERIOD COVERED: Project Final Report FY77–FY81
	6. PERFORMING ORG. REPORT NUMBER:
7. AUTHOR(s): LE Hoff, AR King	8. CONTRACT OR GRANT NUMBER(s):
9. PERFORMING ORGANIZATION NAME AND ADDRESS: Naval Ocean Systems Center, San Diego, CA 92152	10. PROGRAM ELEMENT, PROJECT, TASK AREA & WORK UNIT NUMBERS: PE 24163N, Project X0695-CC (NOSC 814-CM14)
11. CONTROLLING OFFICE NAME AND ADDRESS: Naval Electronic Systems Command, Washington, DC 20360	12. REPORT DATE: 30 March 1981
	13. NUMBER OF PAGES: 54
14. MONITORING AGENCY NAME & ADDRESS *(If different from Controlling Office)*	15. SECURITY CLASS. *(of this report)*: Unclassified
	15a. DECLASSIFICATION/DOWNGRADING SCHEDULE

16. DISTRIBUTION STATEMENT *(of this Report)*

Approved for public release; distribution unlimited.

17. DISTRIBUTION STATEMENT *(of the abstract entered in Block 20, if different from Report)*

18. SUPPLEMENTARY NOTES

19. KEY WORDS *(Continue on reverse side if necessary and identify by block number)*

Ionospheric propagation	Adaptive communications	Signal processing algorithms
Spread spectrum	Equalization	Decision feedback equalization
Serial processors	High-frequency communications	Maximum likelihood sequence estimation
Multipath transmission	Radio antijamming	
Communication models	Computerized simulation	

20. ABSTRACT *(Continue on reverse side if necessary and identify by block number)*

Summarizes the Skywave Communication task. Presents some results of the work on wide-band channel modeling, adaptive equalization, and the field test, which demonstrated that serial modulation spread-spectrum signals can be used to provide reliable communication at hf under multipath conditions.

DD FORM 1 JAN 73 1473 EDITION OF 1 NOV 65 IS OBSOLETE

S N 0102-LF-014-6601

UNCLASSIFIED

SECURITY CLASSIFICATION OF THIS PAGE *(When Data Entered)*

OBJECTIVES

Develop communication signal-processing techniques for hf channels consisting of surface waves and/or skywaves. Address both conventional and spread-spectrum modulation. Develop a wide-band channel model and software simulator. Develop adaptive equalization signal-processing techniques and computer simulation software. Perform an hf experiment to record signals for verifying the channel model and signal-processing algorithms.

RESULTS

1. Computer simulations were developed for four signal-processing algorithms: RAKE, linear equalization, decision feedback equalization (DFE), and maximum likelihood sequence estimation (MLSE). Tests showed that the MLSE performed the best and the linear equalizer the worst; but since the MLSE receiver complexity grows exponentially with multipath dispersion, the DFE was felt to be the best choice for the hf channel. The DFE algorithm was extended to incorporate spread-spectrum demodulation.

2. Processing simulated and field test recorded data demonstrated the application of the DFE to serially modulated signals in the hf band. For best performance, the algorithm had to be configured manually for each channel condition.

3. All algorithms perform poorly when the received signal goes into a deep, flat fade. To counter these fades, a technique such as diversity and/or error detection and correction encoding with interleaving is required.

4. In general, the DFE and MLSE provided for significant improvement in bit error rate on channels with severe multipath. The wide-band spread-spectrum signal usually performed better than the narrow-band non-spread-spectrum signal.

5. The hf channel model of CC Watterson et al was extended to accommodate wide bandwidths by taking into account the delay differences between the ordinary and extraordinary wave and the signal distortion caused by variations of phase delay with frequency.

RECOMMENDATIONS

1. Process the data taken during the FY80 field test to verify the wide-band channel model assumptions.

2. Embed the DFE and MLSE algorithms in a real-time data link system and test it over both short- and long-range hf paths.

CONTENTS

INTRODUCTION

PROJECT OVERVIEW

The Skywave Communication task was initiated in FY77 under the Survivable High-Frequency Communications (SHFC) block program, which was concerned primarily with developing technology to meet the Navy's need for extended task force communications under hostile jamming conditions. In FY80 the task was moved into the High-Frequency Improvement Program (HFIP).

The objective of the Skywave Communications task was to develop communication signal-processing techniques for hf (2–32 MHz) channels consisting of surface waves and/or skywaves. Because of interest in using spread-spectrum modulation for electronic warfare (EW) environments, the task addressed both conventional and spread-spectrum modulation. The approach was (1) to develop a wide-band channel model and software simulator, (2) to develop adaptive equalization signal-processing techniques and computer simulation software, and (3) to perform an hf experiment to record signals with which to verify the channel model and signal-processing algorithms.

The purpose of this final report is to summarize the Skywave Communication task and present some of the results of the work on wide-band channel modeling, adaptive equalization, and field testing. Additional results of tests on the Decision Feedback Equalizer are given in a companion Skywave Communication Techniques document (ref 1).

Figure 1 is a bar chart showing the major emphasis of the Skywave task in each year from its inception. In FY77, when the project was initiated, the major emphasis was on developing a wide-band skywave channel model. The intent was to provide a good understanding of the channel for the purpose of developing adaptive signal-processing algorithms. By the end of FY78 a channel model and software simulator for Skywave signals was completed (ref 2). These outputs proved to be useful tools for the evaluation of the receiver algorithms that were developed later in the program. In FY79 the model and simulator were modified (ref 3) to include the surface-wave and deviative (wave-bending) path losses previously omitted.

The major emphasis shifted in FY78 from hf channel modeling to the development of adaptive signal-processing algorithms for dispersive channels. Both narrow-band (3 kHz) and wide-band (100 kHz spread-spectrum) signal modulations were included. For evaluating the adaptive signal-processing algorithms, two computer simulation programs were developed—one for maximum likelihood sequence estimation (ref 4) with narrow-band signals and the other for decision feedback equalization with narrow-band and wide-band options (ref 5-7).

---

[1]NOSC TD 471 (in preparation), Skywave Communication Techniques: Decision Feedback Equalizer Test Results, by LE Hoff and AR King (1981).

[2]NOSC TR 208, Addendum 1, Hf Channel Simulator for Wideband Signals, by R Lugannani and HG Booker, 6 November 1978.

[3]NOSC TR 208, Hf Channel Simulator for Wideband Signals, by R Lugannani and HG Booker, 31 March 1978.

[4]Adaptive Maximum Likelihood Sequence Estimation for the Hf Channel, by LE Hoff and S Norvell; Conference Proceedings for the 13th Asilomar Conference on Circuits, Systems, and Computers, 5-7 November 1979, held at Pacific Grove CA, IEEE Catalog no 79CHiA68-8C, Library of Congress no 79-88185.

[5]Interim Technical Report, Hf Channel Adaptive Equalization Algorithm, by P Monsen and S Parl, Signatron Inc, Lexington MA, Contract N66001-77-D-0248, December 1977.

[6]Phase I Progress Report, Hf Channel Adaptive Equalization Algorithm, by P Monsen, Signatron Inc, Lexington MA, Contract N66001-77-C-2048, 1 February 1978.

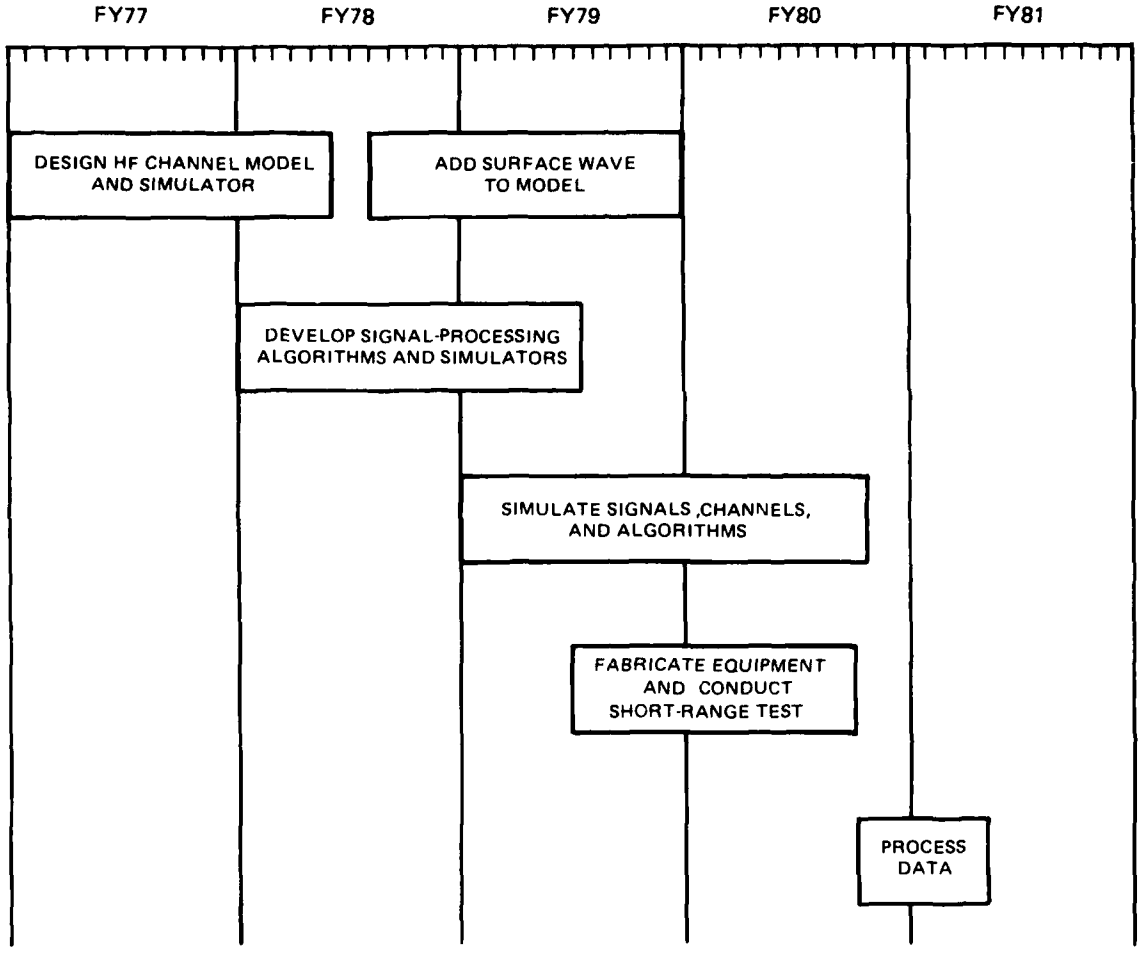

Figure 1. Skywave Communications progress chart.

The fabrication of a data acquisition system was initiated in FY79 in preparation for a field test. The system was designed to be able to transmit, receive, and record narrow-band signals for computer processing. The field test was conducted in California between Pt Mugu and San Diego, an over-water path of about 145 statute miles. The test demonstrated that signals with bandwidths as wide as 100 kHz could be transmitted and received by means of Radio Transmitting Set AN/URT-23(V) (modified for wide-band signals), Antenna Coupler Group AN/URA-38, two whip antennas, a receive multicoupler, and a wide-band Racal receiver (RS6595). Appendix A describes the field test and the data base of signals collected.

[7]Report, Decision Feedback Equalizer Simulation (DFES) Data Base Design, by P Monsen, Signatron Inc, Lexington MA, Contract N66001-77-C-0248, July 1978.

Table 1 lists the four major computer software systems that were developed by the Skywave Communication task. The first is the hf channel simulator developed by R Lugannani and HG Booker under contract with Computer Sciences Corp (ref 2,3). The second is the adaptive equalizer and MLSE simulator software for narrow-band signals, developed by NOSC (ref 4). The third is the spread-spectrum equalizer simulator developed by P Monsen and S Parl, of Signatron Inc (ref 5-7). The fourth is an hf channel evaluation and data analysis program designed by R Lugannani and written by Computer Sciences Corporation. More will be said about the simulation programs in the next two major sections.

Type	For
Hf channel simulator	Narrow-band and wide-band signals
Equalization and MLSE algorithms	Narrow-band 2400-BPS data links
DFB equalization and RAKE algorithms	Spread-spectrum 2400-BPS data links
Wide-band hf channel evaluation and data analysis	

Table 1. Major software systems.

SIMULATION-SYSTEM APPROACH

Figure 2 is a block diagram of an hf communication data link. A mathematical model was developed for the channel and programmed to simulate it in non-real time. A program that simulates the hf channel was designed to accept a digital tape input containing a digital-sampled representation of the transmit information, $\{I\}$, and signal, $S(t)$. The simulator then convolves the input signal, $S(t)$, with the channel response, $h(\tau)$, to create the output signal $Z(t)$, which is stored on digital magnetic tape.

Mathematical algorithms that were developed for processing the received signals to estimate the transmitted bits, $\{\hat{I}\}$, were programmed as part of receiver simulation programs. The programs were designed either to accept digital tape input to provide the channel output $Z(t)$ or to generate hf signals internally. Tape inputs could be from either the hf channel simulator or the hf field test. The simulation program combines $Z(t)$ with noise $N(t)$ to provide the receiver input $Y(t)$. The noise can be provided either from a second magnetic tape or from internally simulated white Gaussian noise. By appropriately combining the signal and noise sources, we can produce input waveforms with predetermined signal-to-noise ratios (SNR).

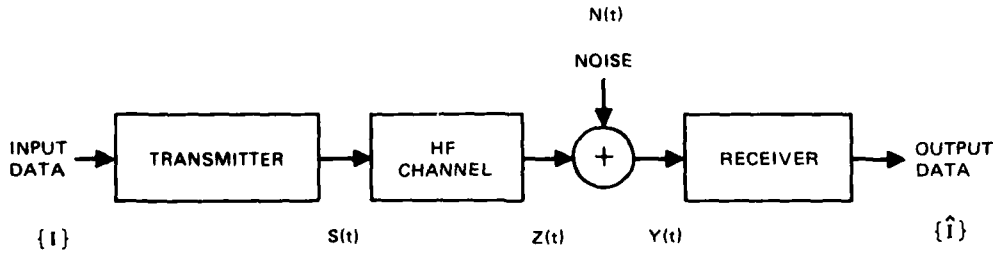

Figure 2. Block diagram of a data communication system.

HIGH-FREQUENCY CHANNEL MODEL

INTRODUCTION TO CHANNEL MODELING

The use of channel simulators to study the performance of communication systems and to assist in their design has become increasingly popular in recent years. By employing a simulator, it is possible to reproduce given channel characteristics as desired for the purpose of comparing different system designs in identical environments.

In the following sections we present a description of a wide-band hf channel model that was used to develop a computer simulation. The channel model presented here is based upon the model proposed and analyzed by CC Watterson (ref 8). It takes into account all ionosphere phenomena that have a significant effect on wide-band communications. Many of these phenomena--such as delay differences between the ordinary and extraordinary waves and signal distortion caused by variations of delay with frequency--were neglected in earlier simulators, with the result that their bandwidths were limited to signals less than 3 kHz wide.

IONOSPHERIC WAVE PROPAGATION

The ionosphere is an upper region of the earth's atmosphere (ref 9,10) that is created by the action of extreme ultraviolet and X-rays from the sun on oxygen and nitrogen molecules, splitting them into free electrons and positive ions. Figure 3, an example of an electron density profile, shows the electron density per cubic metre as a function of height. The ionization starts at about 55 km, increases with altitude to about 250 km, then decreases. The height of maximum density can vary typically from 200 to 400 km depending upon the intensity of the sun's radiation and the recombination rate of the ions.

The ionosphere is formed into layers--primarily the D, E, and F layers. Occasionally the F layer appears to split into two layers termed F1 and F2, but the normal F1 layer does not have a peak intensity of electron concentration and is instead a ledge at the base of the F2 layer. The D layer, which is the lowest, extends from about 55 to 90 km. The ionization in the D layer is too weak to reflect radio signals; therefore the signals pass through it. Because ions in the D region quickly recombine, signals passing through it are attentuated.

Since the ionosphere is created by the sun, it is constantly changing. Its structure exhibits periodic variations of diurnal, annual, and sunspot-cycle length. With respect to a point on the earth's surface, after sunset the D layer disappears and the E layer lasts only a few hours. During the night the E and F layers rise and merge. Ionization is weaker at night than during the day.

Frequencies that reflect from the ionosphere usually are those between 2 and 32 MHz (the hf band). During high sunspot activity, however, frequencies as high as 60 MHz can be reflected.

---

[8]ESSA Technical Report ERL 122-ITS80, Experimental Verification of an Ionospheric Channel Model, by CC Watterson, JR Juroshek, and WD Bensema, July 1969.

[9]National Bureau of Standards Monograph 80, Ionospheric Radio Propagation, by K Davis, 1 April 1965.

[10]Radio Wave Propagation and the Ionosphere, 2nd edition, vol I, by YL Alpert, translated by RB Rodman, Consultants Bureau, New York-London, 1973.

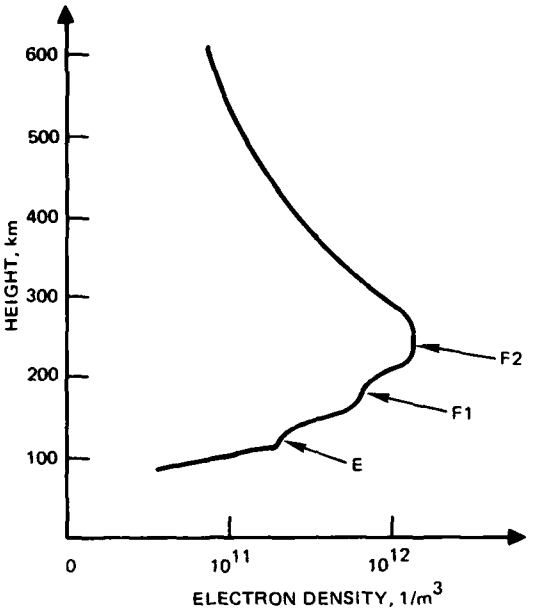

Figure 3. Electron density profile.

Because of the layered structure, the ion density is not uniform with height. At any given frequency (ref 11) the upgoing radio wave (fig 4) penetrates a region of increasing electron density. The ambient electrons in the plasma are forced to oscillate in response to the alternating electric field impressed by the radio waves. The electron oscillation creates an additional electromagnetic field that advances the phase of the radio wave and retards its group velocity. Owing to the repulsion between like charges, an electron displaced from its mean position attempts to vibrate about that position with a plasma frequency (in Hz) of

$$f_p \simeq 9\sqrt{N_e} \quad , \tag{1}$$

where N_e is the concentration of free electrons per cubic metre. As the radio wave approaches the altitude at which its frequency becomes equal to the plasma frequency, the additional electric field begins to approach the amplitude of the incident field and the wave is slowed down and finally reflected.

If, upon vertical incidence, the frequency of the radio wave exceeds the plasma frequency, f_p, the wave is not reflected and passes through the ionosphere. If the radio wave intersects the ionosphere at an angle ϕ as measured from perpendicular, however, the maximum frequency that can be reflected is increased to $f_p \sec \phi$.

[11] High Power Radar Studies of the Ionosphere, by JV Evans, Proceedings of the IEEE, vol 63, no 12, p 1636-1650, December 1975.

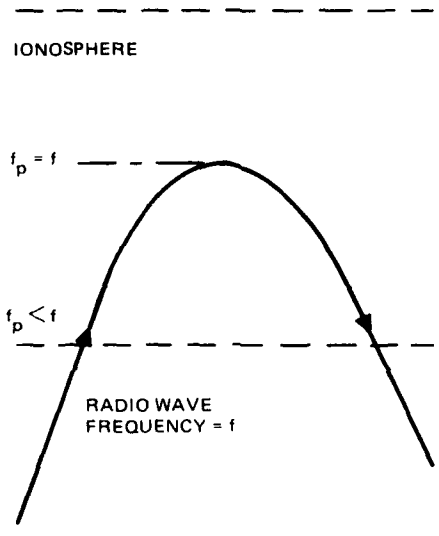

Figure 4. Reflection of a radio wave from the ionosphere.

Long-distance communications can be achieved by obliquely reflecting the waves off the E and F layers. Figure 5 shows the geometry of radio-wave reflection off the E and F layers. If the radio frequency is near the frequency $f_p \sec \phi$, two reflections may occur from the F layer one at a low angle and one at a higher angle. Depending upon the conditions, more than one of the ray traces shown can exist at the same time, causing multiple outputs for every input signal. These outputs are called multipaths because there are multiple paths to the receiving terminal.

As shown in figure 6, radio waves can reflect off the earth or ocean as well as the ionosphere, so that multiple-hop paths are possible. These paths are designated by the number of hops and the layer reflected. For example, a 2-hop reflection from the E layer would be a 2-hop E or simply 2E. Similarly a 2-hop wave from the F2 layer would be a 2F2 wave.

A common method of measuring the ionosphere is to transmit a sequence of pulses on closely spaced frequencies. For each transmitted pulse, there may be several delayed receiver pulses, one for each multipath. By adjusting the propagation delay at the receive terminal and displaying the outputs, we can produce what is called an ionogram. Figure 7 is a sketch of an oblique ionogram that shows the presence of the E and F ionospheric layers and the ordinary (o) and extraordinary (x) propagation modes. Ionograms comprise a useful aid in picking transmission frequencies for long-distance communication links.

NARROW-BAND CHANNEL MODEL

Generally the output of the hf channel consists of delayed replicas of the transmitted signal; therefore an obvious model for the channel consists of a tapped delay line. The taps are located at time delays, τ_ℓ, equal to the path time delays, where $\ell = 1, 2, \ldots, L$ and L is the

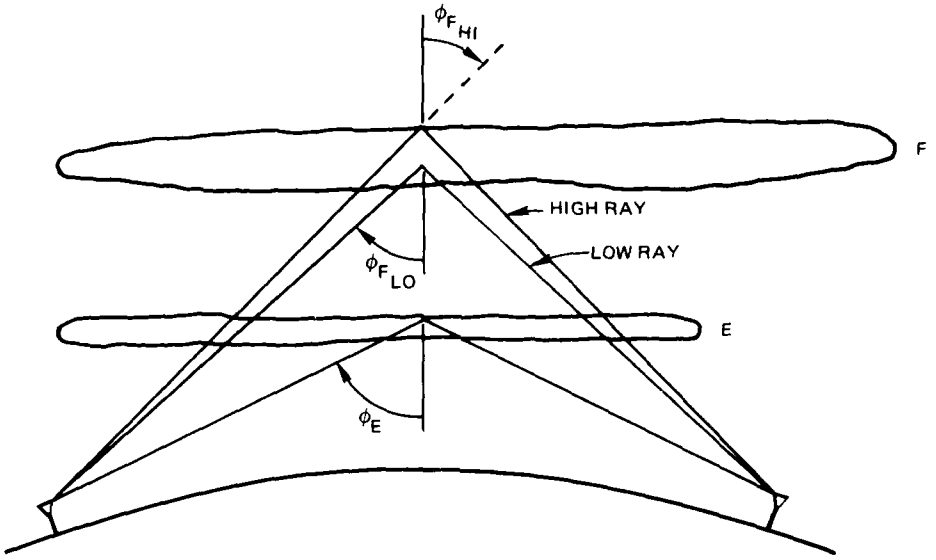

Figure 5. Radio waves obliquely reflecting off the E and F layers.

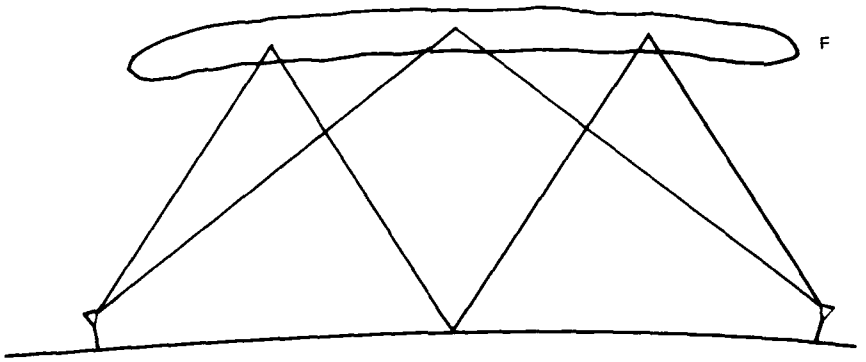

Figure 6. Multiple-hop paths from transmitter to receiver.

number of multipaths. On each tap there is a complex multiplier, α_ℓ, called a tap-gain, which attenuates the amplitude and shifts the phase of the tap output to correspond to the received multipath signal. Figure 8 is a block diagram of the tapped-delay-line model for the hf channel. Because the received multipath signals randomly fade with time, the tap-gains are random processes. The model is specified, therefore, when we give the tap delays and the statistics of the tap-gains.

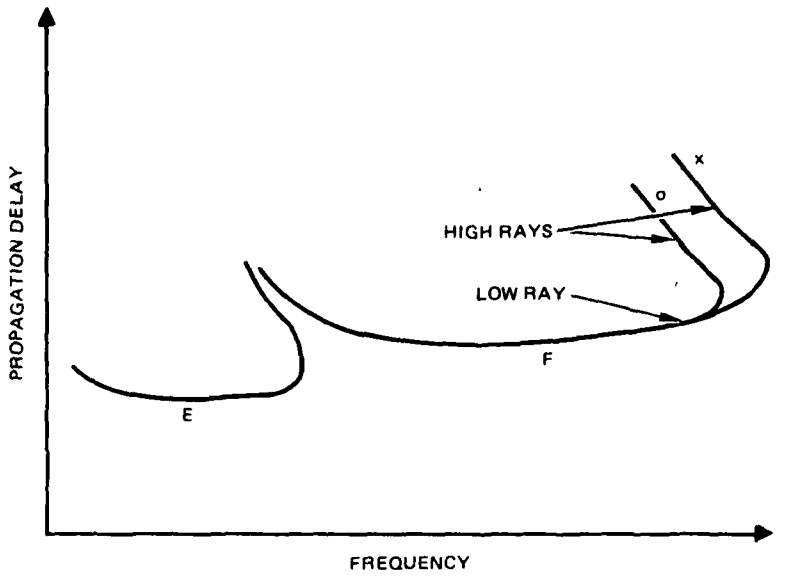

Figure 7. Ionogram.

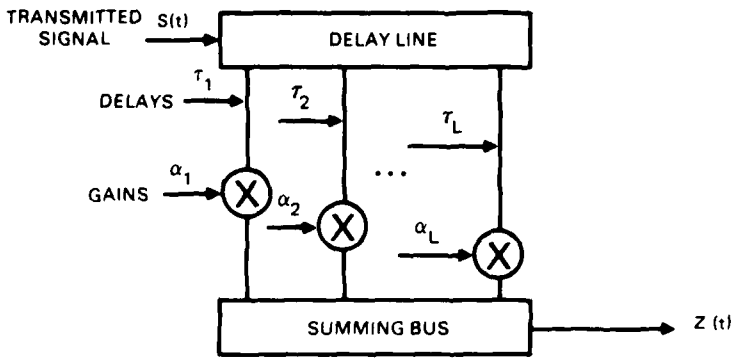

Figure 8. Tapped delay line model.

The wide-band channel model proposed here is based upon the ionospheric channel model proposed and analyzed by Watterson (ref 8). The tap-gain functions are assumed to be independent zero-mean Gaussian random processes. Figure 9 is a sketch of the Gaussian-shaped power spectrum for one of the tap-gain functions. Only two parameters are needed to specify the power spectrum: the mean ν_ℓ and variance σ_ℓ^2. The mean ν_ℓ is called the Doppler shift, and twice the standard deviation, $2\sigma_\ell$, is called the frequency spread.

Although there are many functions that could be used to characterize the input and output waveforms, only two are used. The first is the causal time-varying impulse response $h(\tau,t)$, which is the channel response at time t due to an impulse at time $t-\tau$. The other is

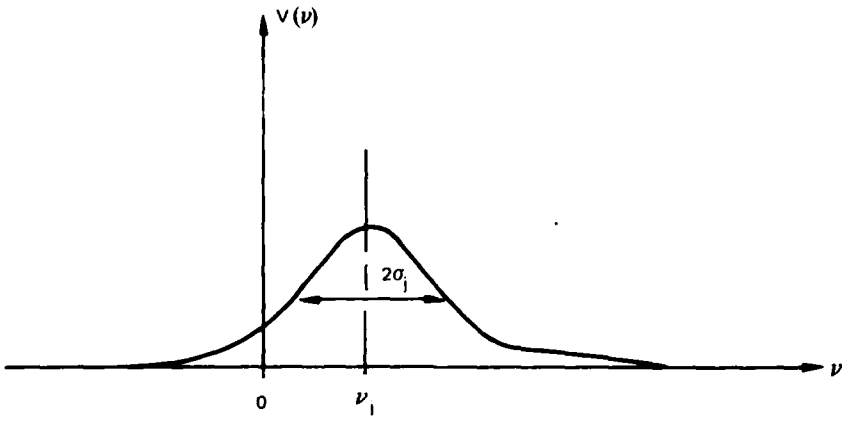

Figure 9. Tap-gain power spectra.

the time-varying frequency response H(f,t), which is the response of the channel to a continuous-wave (cw) signal at time t and frequency f. These functions are related by the Fourier transform on τ:

$$H(f,t) = \int_0^\infty h(\tau, t)\, e^{-2\pi f \tau}\, d\tau \quad . \tag{2}$$

For the tapped-delay-line model in figure 8, the impulse response is as follows:

$$h(\tau,t) = \sum_{\ell=1}^{L} \alpha_\ell(t)\, \delta(\tau - \tau_\ell) \quad , \tag{3}$$

where $\delta(\tau-\tau_\ell)$ is the delta function. The complex time-varying frequency response of this model is

$$H(f,t) = \sum_{\ell=1}^{L} \alpha_\ell(t) \exp\{-i2\pi\tau_\ell f\} \quad . \tag{4}$$

In equations (3) and (4), the subscript ℓ numbers the tap or path, τ_ℓ is the time delay of the ℓ th path, and L is the total number of propagation paths. The tap-gain functions $\alpha_\ell(t)$, with $\ell = 1, 2, \ldots, L$, are complex random processes that change the amplitude and phase of the

transmitted signal. In our model, the tap-gain functions are assumed to be independent complex Gaussian random processes. A number of experimenters (ref 8, 12-14) have made measurements on hf channels and have shown that this assumption is reasonable.

As an example of a multipath channel, figure 10 shows a tapped-delay-line model of a two-path channel. The voltage gains for the two paths are a_1 and a_2. The phase shifts and time delays are θ_1, θ_2, and τ_1, τ_2 respectively. What are important, however, are the relative phase shift

$$\Delta\theta = \theta_2 - \theta_1 \tag{5}$$

and relative time delay

$$\Delta\tau = \tau_2 - \tau_1 \quad . \tag{6}$$

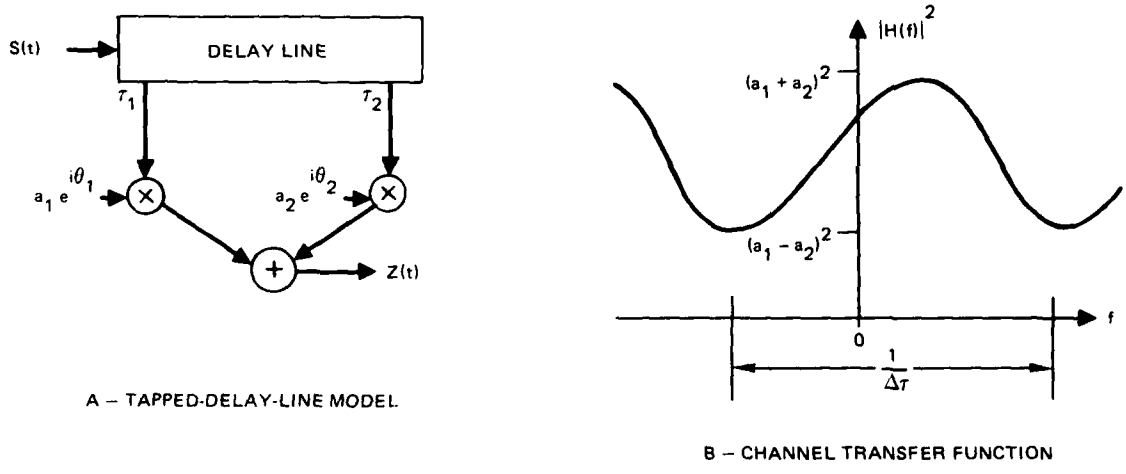

Figure 10. Model and transfer function of channel with two paths.

[12] Communication Systems and Techniques, by M Schwartz, W Bennett, and S Stein, p 355, McGraw-Hill, New York, 1966.

[13] Evaluation of a Gaussian Hf Channel Model, by HN Shaver, BC Tupper, and JB Lomax, IEEE Transactions on Communication Technology, vol COM-15, no 1, p 79-85, February 1967.

[14] Correlation Measurements on an Hf Transmission Link, by F David et al, IEEE Transactions on Communication Technology, vol COM-17, no 2, p 245-256, April 1969.

The squared amplitude of the transfer function for a given set of parameters is given by the expression

$$|H(f)|^2 = a_1^2 + a_2^2 + 2\, a_1\, a_2 \cos(2\pi f \Delta\tau + \Delta\theta)\,. \tag{7}$$

On fading channels, the values of a_1, a_2, and $\Delta\theta$ change with time, so that the transfer function will also change. In this model, a_1 and a_2 change independently. When a_1 equals a_2, the spectrum has nulls separated by $(\Delta\tau)^{-1}$ hertz. If the pulse bandwidth is greater than $(\Delta\tau)^{-1}$, there will be severe distortion. However, for pulses much longer than the multipath spread, the bandwidth will be much less than $(\Delta\tau)^{-1}$ and the distortion will be minor.

Doppler is another example of signal distortion caused by the channel. Shown in figure 11 is a two-path example consisting of the surface wave and the Doppler-shifted skywave. If we transmit long tones, we get a beat note between the two paths, evidenced by fading. If the paths have equal strength, the resultant envelope could fade to zero, causing high error rates.

WIDE-BAND CHANNEL MODEL

The narrow-band channel model that we have presented assumes that the signals from individual modes are not distorted and that the channel output is a direct summation of delayed and weighted versions of the transmitted signal. Watterson (ref 8) concluded

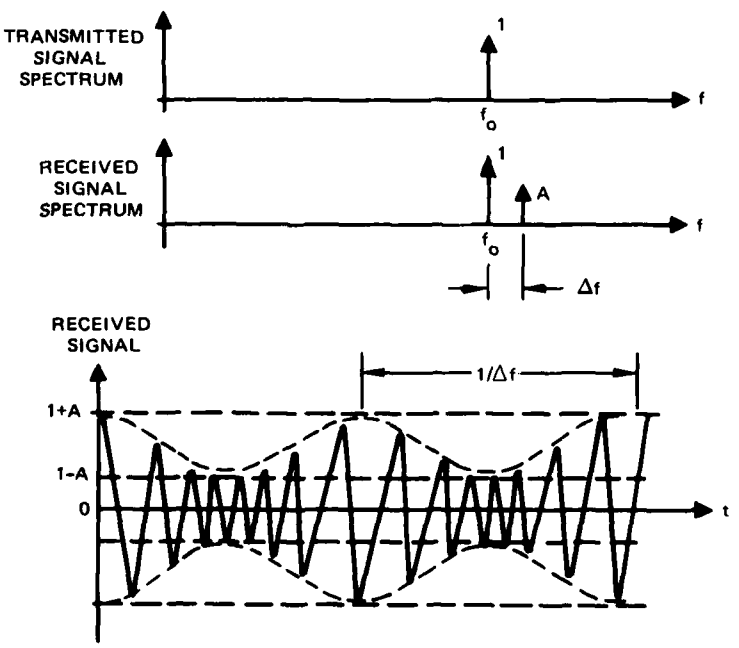

Figure 11. Two-path channel with differential Doppler.

that that model was good for bandwidths up to 2.5 kHz at night and 10 kHz during the day. Wider bandwidth signals, however, become distorted. We can see this from the ionogram in figure 7: if the path propagation delays versus frequency were horizontal lines, all frequencies would be delayed the same. Each delayed signal is undistorted provided the path loss is uniform across the frequency band. But the curves of path propagation delays versus frequency are not straight lines; they exhibit considerable bending at the low and high frequencies for each path. Also, the path loss is in general nonuniform.

To derive a wide-band model, it was assumed that (1) the distortion is caused by phase delay variations across the band and (2) the distortion is deterministic and time invariant for the duration of the message.

The transmitted signal, s(t), is related to its spectrum S(f) by the Fourier transform

$$s(t) = \int_{-\infty}^{\infty} S(f) \exp [2\pi i f t] \, df. \tag{8}$$

More or less distorted versions of this signal are received depending on the ray path – ie, E-region or F-region, ordinary or extraordinary, high or low angle. Distortion of signals reflected from the ionosphere has been studied by several authors, who have attempted to characterize the impulse response for a simplified model of the ionosphere (ref 15–19). Unfortunately, these results have been derived by means of ionosphere models that are too idealized for our purposes, and the impulse responses obtained are too complicated for easy implementation. To obtain tractable expressions for the distortion, we shall assume that it is caused primarily by the fact that the delay is a function of frequency and is not constant across the signal bandwidth. This characterization of the distortion mechanism allows us to make a number of approximations that result in relatively simple expressions for the distorted signal.

Let f_c denote the carrier frequency and let $\tau_j(f)$ denote the delay of the jth path as a function of frequency. It follows from equation (8) that the distorted baseband signal returned from the ionosphere is given by the expression

---

[15] The Impulse Response of a Cold Stratified Plasma in the Presence of Collisions and a Vertical Magnetic Field by a Multiple-Scattering Technique, by KG Gray and SA Bowhill, Radio Science, vol 9, p 559-566, 1974

[16] Transient Response of Stratified Media: Multiple-Scattering Integral and Differential Equations for an Impulsive Incident Plane Wave, by KG Gray and SA Bowhill, Radio Science, vol 9, p 57-62, 1974.

[17] Transient Response of Stratified Media: Response to an Arbitrary Incident Plane Wave, by KG Gray and SA Bowhill, Radio Science, vol 9, p 63-69, 1974.

[18] An Integral Equation for the Transient Response of a Stratified Magnetoplasma, by KG Gray, IEEE Transactions on Antennas and Propagation, vol 24, p 539-541, 1976.

[19] Theory of the Electromagnetic Transient Response of the Ionosphere for Plane Wave Excitation, by DA Hill and JR Wait, Pure and Applied Geophysics, vol 90, p 169-186, 1971.

$$Z_j(t) = \int_{-\infty}^{\infty} S(f) \exp\left[-2\pi i (f_c + f) \cdot \tau_j (f_c + f)\right] \cdot \exp\left[2\pi i f t\right] \, df . \qquad (9)$$
$$j = 1, \ldots, N$$

We will characterize this distortion by the coefficients in the power series expansion of the delay about the carrier frequency. This series appears as

$$\tau_j(f_c + f) = \sum_{k=0}^{\infty} \frac{f^k}{k!} \tau_j^{(k)}, \qquad j = 1, \ldots, N \qquad (10)$$

with

$$\tau_j^{(k)} = \frac{d^k}{df^k} \tau_j (f_c + f) \Big|_{f=0} . \qquad (11)$$

Substituting this series into the exponential delay term in equation (9), we obtain

$$\exp\left[-2\pi j (f_c + f) \cdot \tau_j (f_c + f)\right] = \exp\left[-2\pi i \sum_{k=0}^{\infty} f^k D_j^{(k)}\right], \quad i = 1, \ldots, N \qquad (12)$$

where we have defined

$$D_j^{(o)} = f_c \tau_j^{(o)} \qquad j = 1, \ldots, N \qquad (13)$$

and

$$D_j^{(k)} = \frac{1}{k!} \left[k\tau_j^{(k-1)} + f_c \tau_j^{(k)}\right], \qquad k = 1, 2, \ldots \quad j = 1, \ldots, N \qquad (14)$$

Thus for $Z_j(t)$ we have

$$Z_j(t) = \exp\left[-2\pi i D_j^{(o)}\right] \int_{-\infty}^{\infty} S(f) \exp\left[-2\pi i \sum_{k=2}^{\infty} f^k D_j^{(k)}\right]$$
$$\cdot \exp\left[2\pi i f (t - D_j^{(1)})\right] df. \qquad j = 1, \ldots, N \qquad (15)$$

For computational reasons it is convenient to separate the phase and delay terms from the actual distortion of the signal. To this end we define a function $Z_j(t)$ as follows:

$$Z_j(t) = \exp\left[-2\pi i D_j^{(o)}\right] \hat{Z}_j \left[t - D_j^{(1)}\right], \qquad j = 1, \ldots, N \qquad (16)$$

where

$$\hat{Z}_j(t) = \int_{-\infty}^{\infty} S(f)\, H_j(f) \exp\,[2\pi i f t]\, dt\,, \quad j = 1, \ldots, N \tag{17}$$

with

$$H_j(f) = \exp\left[-2\pi i \sum_{k=2}^{\infty} f^k D_j^{(k)}\right]. \quad j = 1, \ldots, N \tag{18}$$

In practice it is convenient to determine $\hat{Z}_j(t)$ by performing a time domain convolution rather than by evaluating the Fourier transform as in equation (17). If the impulse response determined by $H_j(f)$ is denoted by $h_j(t)$, we have

$$h_j(t) = \int_{-\infty}^{\infty} H_j(f) \exp\,(2\pi i f t)\, df, \qquad j = 1, \ldots, N \tag{19}$$

and the desired convolution appears as

$$\hat{Z}_j(t) = \int_{-\infty}^{\infty} s(t-u) h_j(u)\, du. \qquad j = 1, \ldots, N \tag{20}$$

We can see that the phase delay distortion term $D_j^{(o)}$ is the phase of the jth path, $D_j^{(1)}$ is the time delay due to propagation, and terms $D_j^{(k)}$, where $k = 2, 3 \ldots$, represent distortion of the received signal.

Figure 12 is a block diagram of the wide-band channel model. The main difference between the wide-band model and the narrow-band model (fig 8) is the delay distortion filter $H_j(f)$ on each of the taps representing skywave signals.

FUTURE WORK

In deriving the wide-band hf channel model above it was assumed that (1) distortion to individual signals from the ionosphere was caused by phase delay variations across the band and (2) the distortion was deterministic and time invariant for the duration of the message. To establish time periods and bandwidths for which these assumptions provide a reasonable model, a field test was conducted in which signal distortion was recorded and measured. Although a single field test does not establish a general principle, it can provide a sample of reality and a measure of credibility to the model.

During the FY80 Skywave Communication field test, wide-band signals were transmitted in California from Pt Mugu to San Diego and the received signals were recorded. Some of these signals were specifically designed for probing the ionosphere and measuring parameters that were used in the wide-band channel model. (A more detailed description

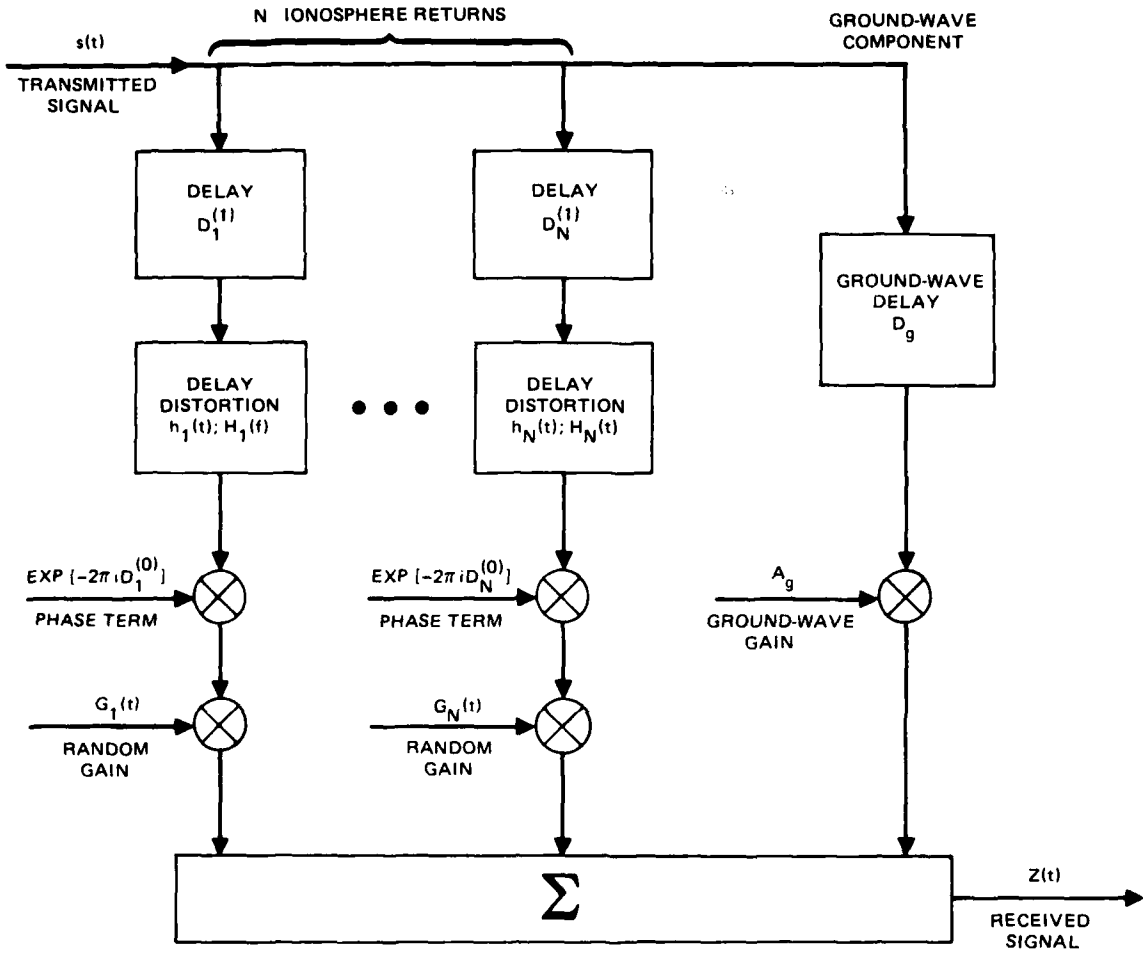

Figure 12. Block diagram of wide-band hf channel model.

of the field test and data are given in appendix A.) The measurements were to be made by means of computer analysis. A computer program was developed by CDC that would measure propagation mode dispersion as well as estimate the channel time-variant parameters. Currently the program is designed to run under self-test conditions for program exercising and demonstration of its capabilities. As of this time the program has not been modified to accept field test tapes as input. The next steps would be to modify the program to accept field test data, to verify proper performance, and to analyze the skywave signals recorded during the Pt Mugu to San Diego tests.

ADAPTIVE EQUALIZATION

The primary objective of the Skywave Communications task was to develop adaptive signal processing techniques for hf channels consisting of time-variant multipath signals. Considerable research during the last 15 years (ref 20, 21) has been directed toward improving communications reliability on slowly time-varying channels. Impressive gains have been accomplished on channels such as troposcatter (ref 22–24) and telephone lines (ref 21). Little has been done at hf, however, since the early work of DiTorro (ref 25). The primary differences between hf channels and these other channels are faster fade rates, longer multipath spreads, and variable channel mode structures. In addition, previous research on adaptive equalization techniques has not been applicable to spread-spectrum modulation. Our approach has been to explore these techniques and extend them to the hf channel and spread-spectrum signals.

First we give an overview of signal techniques used for multipath dispersive channels. We start by reviewing the communication problem of making bit-by-bit decisions for a multipath channel, then we describe the signal-processing techniques. Simulation results for a nonfading multipath channel are presented to show the relative performance of several of these techniques.

Following the overview, we discuss the decision feedback equalizer (DFE). We present the signaling scheme and receiver processing algorithm in greater depth. Finally, we present simulation and field test results for the DFE algorithm.

OVERVIEW OF TECHNIQUES FOR COPING WITH MULTIPATH CHANNELS

As shown in figures 5 and 6, several propagation paths may exist between transmitter and receiver. Because of the differences in path length, the output from the channel consists of the sum of delayed echoes. The time-of-arrival difference of the echoes constitutes time dispersion. For long distances (several thousand miles) the dispersion can be 7 or 8 ms. During the Skywave Communication Field Test (ref 26) between Pt Mugu and San Diego

---

[20] Advances in Equalization for Intersymbol Interference, by JG Proakis, paper published in Advances in Communication Theory, edited by Balikrisman and Viterbi, Academic Press, New York, 1975.

[21] A Survey of the Communication Theory Literature, 1968–1973, by RW Lucky, IEEE Transactions on Information Theory, vol IT-19, no 5, November 1973.

[22] High Speed Modem for Troposcatter, by P Monsen, EASCON, Washington DC, October 1974.

[23] Adaptive Equalization of the Slow Fading Channel, by P Monsen, IEEE Transactions on Information Theory, vol COM-22, no 8, August 1974.

[24] Theoretical and Measured Performance of a DFE Modem on a Fading Multipath Channel, by P Monsen, IEEE Transactions on Communications, vol COM-25, no 10, October 1977.

[25] Communication in Time-Frequency Spread Media Using Adaptive Equalization, by MJ DiTorro, Proceedings of the IEEE, vol 56, no 10, October 1968.

[26] NOSC TD 309, Hf Skywave Communications Test Plan, by GP Francis, November 1979.

(145 miles), time spreads up to 8 ms were observed. This time dispersion of the received signal causes individual pulses of digital data streams to interfere with pulses that follow them. For example, a binary serial bit-stream with a data rate of 2400 bits per second would have pulse widths of about 417 μs. If the channel disperses the pulse to span 8 ms, then each transmitted pulse could interfere with the following 20 pulses.

The multipath problem at hf has been understood for quite some time, and a number of techniques have been developed for minimizing the effects on error rate. Current hf modems use long pulse durations to minimize received-signal distortions, then they adjust to the higher data rates by sending parallel tones (serial bit-streams on adjacent frequencies). Figure 13 shows the basic concept behind the use of long pulse durations. By using pulse durations much longer than multipath time spread, pulse distortion is confined to the leading and trailing edges of the pulse. By using an undistorted time slice from the center of the received pulse, the receiver can make bit decisions free of intersymbol interference. But other distortions can occur in the hf channel—selective fading, dispersion, and Doppler shifts—and these distortions continue to cause high error rates. Communication system engineers have used diversity and coding techniques to overcome these difficulties, but the resulting systems have proven to be both expensive and inefficient. Any efficient method employed to cope with these types of time-variant interferences must include some means of measuring and tracking the channel response and some method of adapting the receiver structure to the channel response.

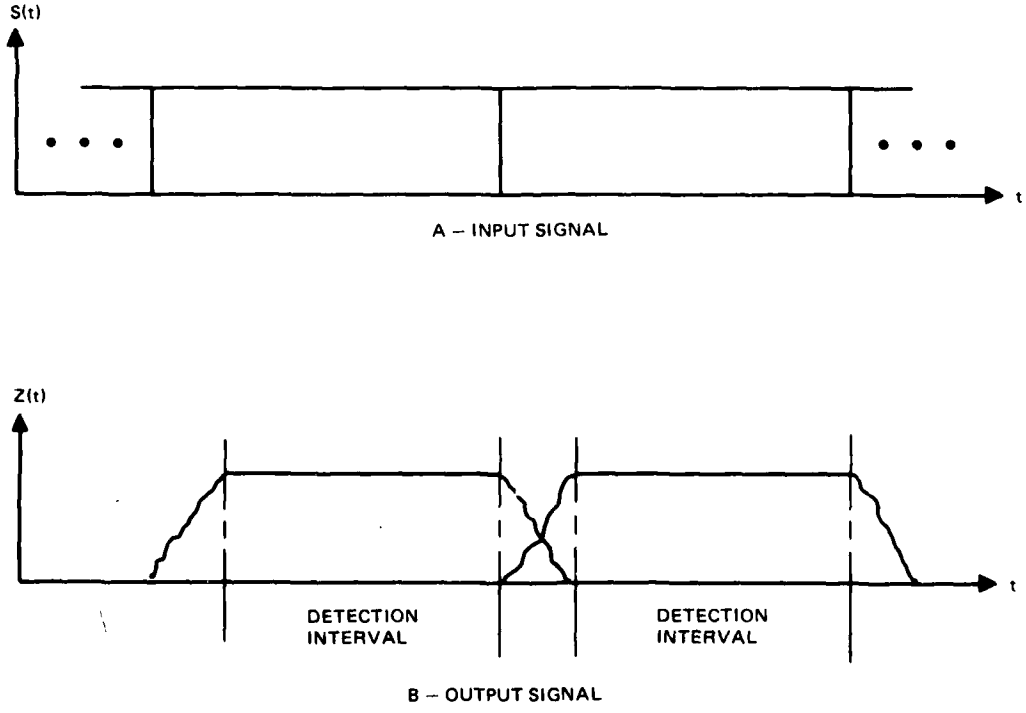

Figure 13. Long pulse durations for multipath channels.

Table 2 lists some of the techniques that have been developed for coping with multipath channels. The paralleled tone differential quadrature phase shift key (DQPSK) modulation scheme is considered a standard for the hf channel (ref 27). The Link-11 and the Navy standard Radio Set AN/URC-88 are based upon this modulation format.

The RAKE system (ref 28-30) uses a wide-band serial spread-spectrum signal. The receiver adaptively tracks the channel pulse response and match-filters the channel output waveform. By match-filtering the channel output, the receiver coherently combines all the multipath signals, thus maximizing the output SNR and minimizing the probability of error. Since the RAKE technique does nothing to minimize or compensate for intersymbol interference, it is mainly applicable to low data rates (less than 200 bits per second).

The linear equalizer was developed by DiTorro (ref 25) and Lucky (ref 21) for the hf band and telephone channels respectively. The channel is treated as a linear filter with frequency and phase distortion. The receiver is designed to filter the signal in such a way as to minimize the mean square error between the filter output and the transmitted signal. Thus, signal fidelity is the optimization criterion for the receiver design.

Technique	Concept	Remarks
Paralled tone DQPSK modulation	Long bauds on adjacent frequencies–nonadaptive	Selective fading causes high error rates
RAKE	Pulse matched filter	Good for low data rates
Linear equalization	Minimize distortion by filtering the received signal	Severe multipath causes high error rates
Decision feedback equalization	Minimize distortion by filtering the received signal and past decisions	Tracking problem
Maximum likelihood sequence estimation	Message matched filter	Exponential growth with pulse spread Tracking problem

Table 2. Summary of signal-processing techniques for multipath channels.

[27] Report CTR-140, Predicted Wave Signalling (Kineplex), by AA Collins and ML Doelz, Collins Radio Co, 20 June 1955.

[28] A Communication Technique for Multipath Channels, by R Price and PE Green Jr, Proceedings of the IRE, vol 46, p 555-570, March 1962.

[29] Technical Report 258, Error Probabilities for Adaptive Multichannel Reception of Binary Signals, by R Price, MIT Lincoln Laboratory, 23 July 1962.

[30] Technical Memorandum 65, An Antimultipath Communication System, by R Price and PE Green Jr, MIT Lincoln Laboratory, 9 November 1956.

Figure 14 is a block diagram of a transversal filter, which becomes a linear equalizer when the tap gains are adjusted to minimize the distortion between the filter output $\hat{I}_n$ and the transmitted bit I_n. The distortion function used here is mean square error, given by the equation

$$J(C) = \min_{\underline{C}} E\left[|I_n - \hat{I}_n|^2 \right] , \tag{21}$$

where $E\left[|I_n - \hat{I}_n|^2\right]$ is the expected value. The optimization of the above quadratic function, which can be performed by applying the Wiener filtering technique, is of the form

$$\underline{C} = \underline{A}^{-1}\,\underline{B} , \tag{22}$$

where $\underline{A}$ is a covariance matrix with element a_{ij} given by the equation

$$a_{ij} = E\left[Y^*_{n-i}\, Y_{n-j} \right] \tag{23}$$

and $\underline{B}$ is a vector with elements

$$b_i = E\left[I_n\, Y^*_{n-i} \right] . \tag{24}$$

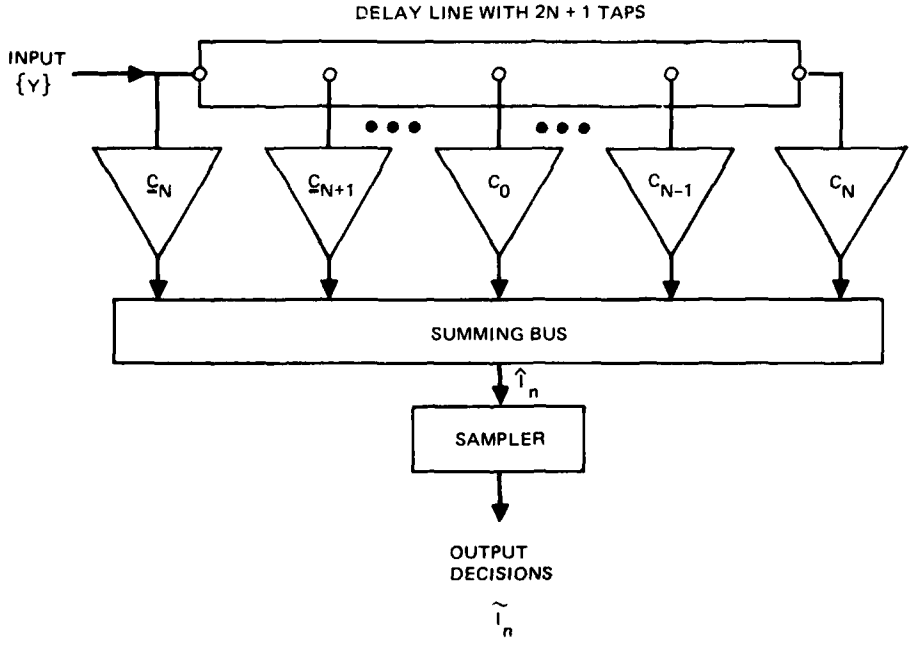

Figure 14. Transversal filter.

The receiver would have to compute the vectors $\underline{A}$ and $\underline{B}$ for each bit and could do this only if it had prior knowledge of the channel and noise statistics.

A simple iterative procedure for determining $\underline{C}$ is to use the method of steepest descent. Figure 15 shows that for a typical tap gain, the mean square error is a quadratic function of the tap gain value and therefore contains a global minimum. An iterative procedure would be to start the equalizer with the tap gains set at an arbitrary initial value. At each iteration the value of the tap gain is adjusted for the n + 1 time by the relationship

$$\underline{C}_{n+1} = \underline{C}_n - \Delta\, \underline{g}_n \,, \tag{25}$$

where Δ is a step size and $\Delta\, \underline{g}_n$ is the slope of the curve at the point of C_n. However, the gradient vector, $\Delta\, \underline{g}_n$, is difficult to determine since it depends on the characteristics of the channel. To overcome this difficulty, Widrow and Hoff (ref 31) have suggested using a noisy estimate of the gradient vector. By using this procedure, the iterative algorithm for adjusting the tap gain coefficients becomes

$$\underline{C}_{n+1} = \underline{C}_n - \Delta\, \underline{g}_n \,, \tag{26}$$

where we compute g_n by the equation

$$\hat{g}_n = -(I_n - \hat{I}_n)\, \underline{Y}_n^* \,. \tag{27}$$

The linear equalizer was found to be effective on communication channels with minor time dispersion (like the telephone channel), but it could not handle the severe time dispersion of

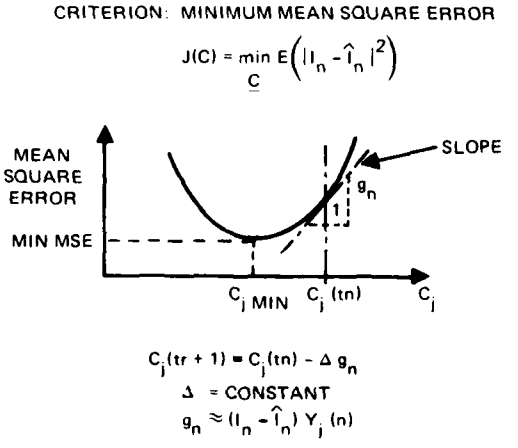

Figure 15. Steepest descent algorithm.

[31] Adaptive Switching Circuits, by R Widrow and M Hoff Jr, IRE WESCON Conv Rec pt 4, p 96-104, 1960.

the hf channel. Multipath spreads longer than one pulse width could cause very high error rates at the output of the equalizer. To overcome this problem, the decision feedback equalizer was developed to utilize both future symbol interference data and past decision data. This technique was successfully applied to the troposcatter channel (ref 22). Figure 16 compares the block diagrams for the linear equalizer and decision feedback equalizer.

In deriving the MLSE algorithm (ref 4), the channel is treated as a linear convolutional waveform encoder. The receiver that minimizes the probability of a message error is the maximum likelihood receiver. This receiver consists of a filter matched to the channel output response and a waveform decoder based upon the Viterbi convolutional decoding algorithm. It is assumed that the channel response is known and time invariant. Under NOSC IR-IED task "Maximum Likelihood Sequence Estimation for the Hf Channel" (ref 4) it was shown that signal processing techniques could be used to estimate and track the channel response with minor loss in performance. A serious problem is that the Viterbi algorithm computation complexity grows exponentially with the ratio of channel time-dispersion width to bit duration. Since time dispersion on the hf channel is commonly several milliseconds long, MLSE receivers may be unrealistic for bit rates of 2400 bits per second or higher.

Figure 17 gives the bit error rate versus the ratio of received signal bit energy to noise density for the equalizer and the MLSE receiver. The channel consists of two paths of equal strength separated by two bit intervals (826 μs). For this comparison the paths are nonfading. The linear equalizer did very poorly because this channel has a very deep null in the passband of the signal. The equalizer tries to compensate for the deep null by applying large gain to those frequencies. Thus the noise on those frequencies is greatly enhanced, causing the bit error rate to remain high. The decision feedback equalizer appears to be free of this problem and performs within 6 dB of the channel that has no intersymbol interference. The MLSE performed the best, almost as good as though there were no intersymbol interference. Because of the exponential growth of the MLSE, the DFE was selected as the best candidate for application to hf spread-spectrum signals.

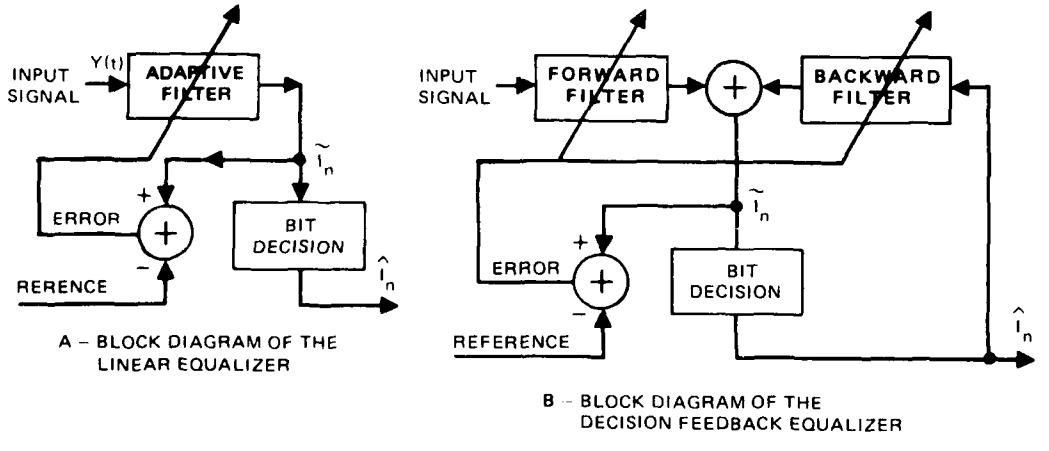

Figure 16. Comparison of the linear and decision feedback equalizers.

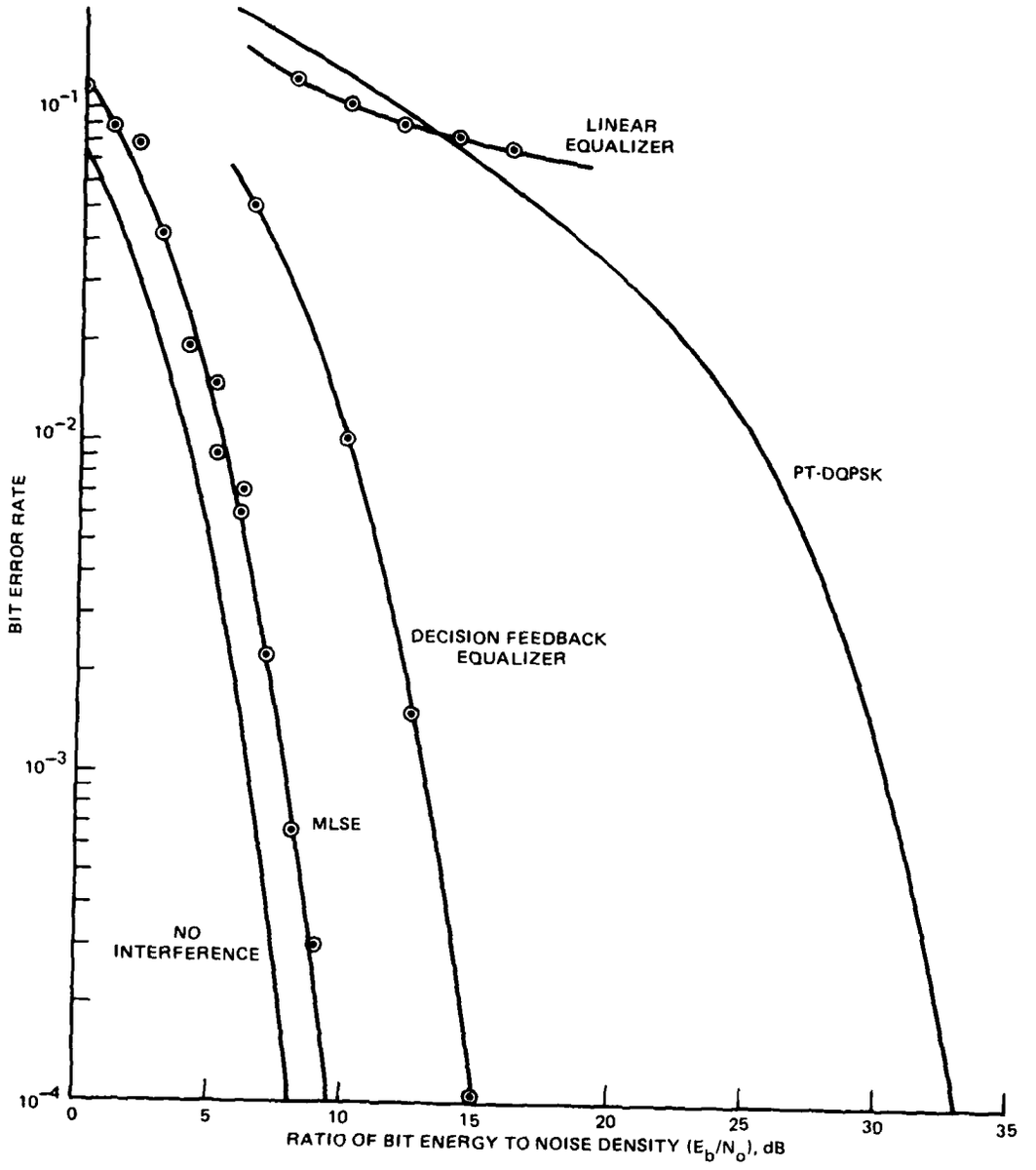

Figure 17. Simulation results of binary signaling through a time-invariant multipath channel.

DECISION FEEDBACK EQUALIZATION (DFE) DESCRIPTION

To program a computer simulation of the adaptive signal-processing algorithm, we had to be specific about the signal waveform out of the transmitter. Figure 18 shows the message format. A serial stream of 4PSK-modulated chips was used as the basic signal, where the digital modulation sequence is completely known by the simulation system. The signal waveform is partitioned by the operator into three parts: a preamble, a training sequence, and a message text. The preamble is used to detect the presence of a signal, estimate the channel output pulse response, and synchronize the receive system to the incoming signal. The training sequence is used for initial training of the adaptive equalizer. During the message text, a reference is transmitted in quadrature with the information for use in tracking the channel response and updating the equalizer tap-gains. The basic data rate for the signal is 2400 bits per second of user information plus 2400 bits per second of reference information. Each symbol is 416.7 μs long and QPSK modulated.

The spectrum of each symbol can be expanded to occupy a larger bandwidth by transmitting several chips per symbol. The number of chips per symbol can be varied from 1 to 40, and the nominal bandwidth will vary from 2.4 kHz to about 96 kHz. Each chip is QPSK modulated, so that there is no obvious change in the signal waveform to indicate the beginning of symbols, training sequence, or message text.

Figure 19 is a block diagram of the DFE circuit described in reference 5. The structure utilizes a forward filter to reduce future digit intersymbol interference and a backward filter to remove past digit intersymbol interference. The DFE receiver must also include the provision for spread-spectrum compression as well as bit synchronization. The tap gains for the forward and backward filters are estimated by means of the LMS algorithm.

The spread spectrum increases the circuit complexity as follows:

The forward and backward filter tap spacing are $Tc/2$ and Tc, respectively, rather than the bit duration T.

The forward and backward filter outputs are compressed before summing.

The bit decision, $\hat{I}_k$, is remodulated with the spread-spectrum sequence for the backward filter.

The forward and backward tap gains are updated at the bit rate, ie every T seconds.

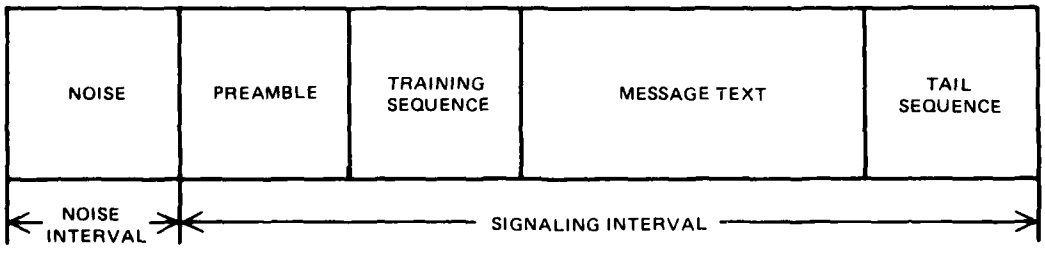

Figure 18. Message format.

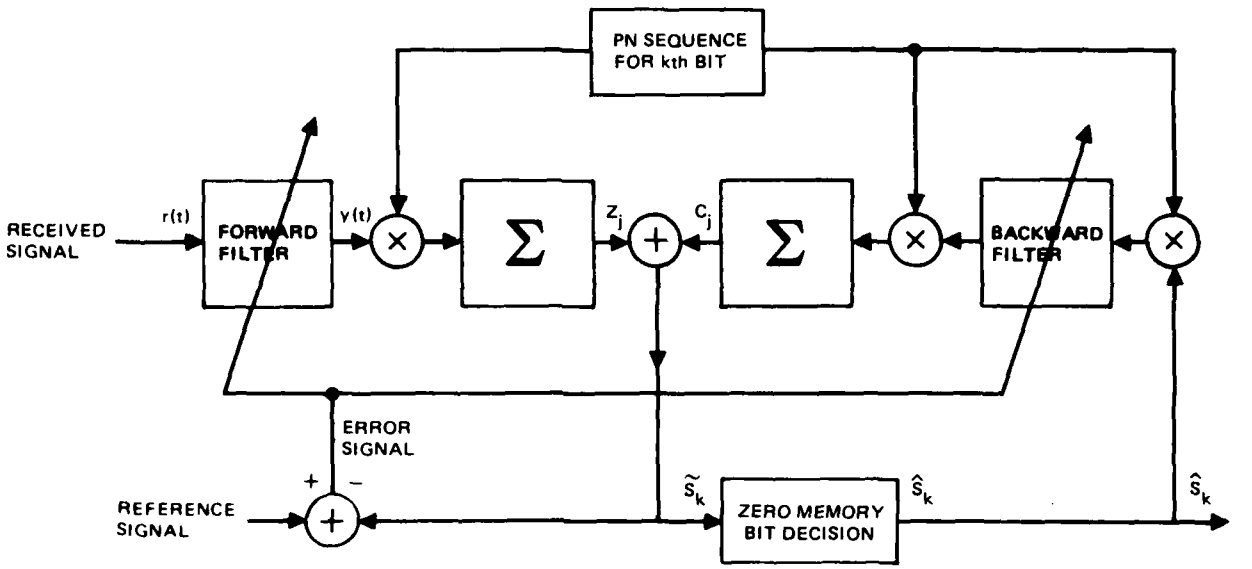

Figure 19. DFE circuit diagram for spread-spectrum modulated signals.

The DFES computer program is an independent simulation tool for evaluating the performance of an adaptive equalization system for the hf channel. The modulator includes the functions of differential encoding, time division multiplexing of reference information, PSK modulation, band spreading, and transmitter filtering. The demodulator contains a filter interpolator, noise filter, PSK demodulation, bandwidth compression, adaptive processor functions, differential decoding of detected data, reference extraction, and bit error rate estimations. The simulation of the hf channel in the DFES is accomplished with a tapped delay line structure with tap gains corresponding to the gain of individual hf paths.

The signal-processing receiver accepts an input binary data sequence transmitted over a time- and frequency-dispersive hf channel (generated either internally or by means of an external magnetic tape), processes the received signal, and outputs a decision of what was sent. The information bits are coded as either 2PSK or 4PSK. The band-spreading technique employed is direct sequence/pseudonoise modulation with 4PSK chips with from 1 to 40 chips per information symbol. The spread-spectrum gain expressed as a bandwidth expansion factor is a variable from 0 to 16 dB. The adaptive portion of the receiver consists of a noise filter and the forward and backward filters of the DFE. The receiver also includes synchronization. The forward and backward filters of the DFE are adapted by either the least mean squares algorithm or the more rapid Kalman/Godard algorithm. The adaption is directed by the use of either receiver decisions (decision-directed, DD) a time-division multiplexed known PN sequence (reference-directed, RD), or a combination of the two (RD/DD).

The receiver alternatives are summarized as follows:

Modulation format	–	2PSK or 4PSK
Receiver type	–	DFE with optional noise filter

Spread-spectrum gain	–	Variable from 0 to 16 dB
Adaption algorithm	–	LMS, Kalman, RAKE, fixed
Adaption direction	–	Decision, reference

Figure 20 is a block diagram of the simulated communication system. At the transmit end, information and reference bits are time-division multiplexed (TDM) in a source generator to produce an output source stream, D. The differential encoder converts the source digits into sequence A. If a reference is transmitted, the differential encoder is not used. The spread-spectrum coder converts each bit symbol, A_k, into a sequence of chip symbols, $\{\alpha_i^k\}$, where each chip symbol is defined according to the formula

$$\alpha_i^k = A_k P_i \quad ,$$

and P_i is the pseudorandom chip value selected from the set

$$\{1,-1,j,-j\} \quad .$$

The transmit modulator generates a complex representation of a sampled data waveform. The channel converts the modulator output, Q, into a sampled data sequence, R, by means of a transversal filtering operation. Zero-mean complex Gaussian noise samples are added to the channel output to provide the equivalent receiver input.* The first receiver function is to filter and resample the input at the receiver sampling rate (RSR). The complex samples, S,

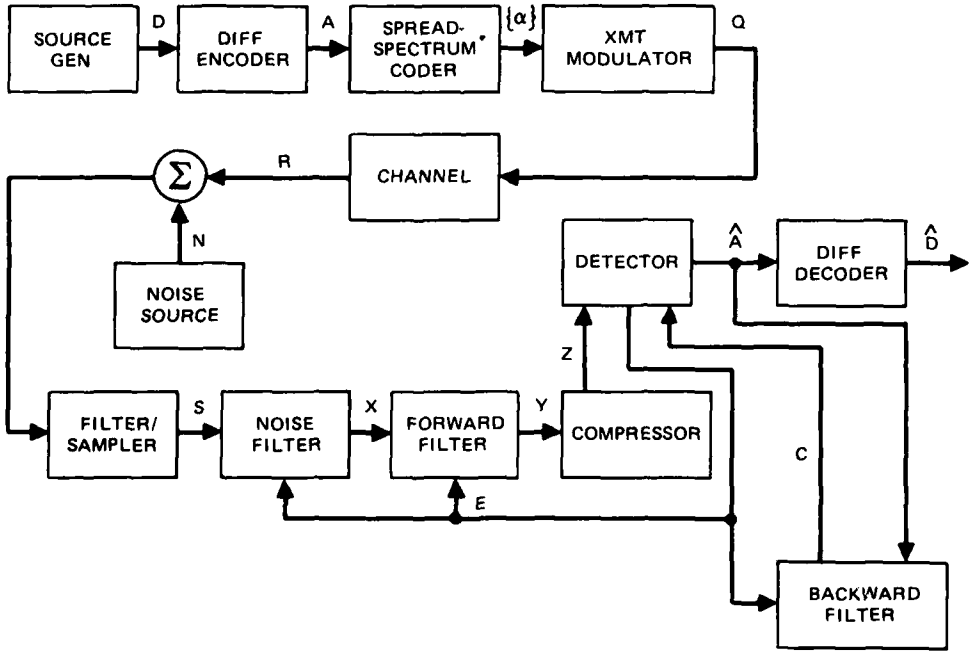

Figure 20. Communication simulation system block diagram.

*Simulation tests can use real hf noise from magnetic tape as well as internally generated Gaussian noise.

are filtered by a noise filter to minimize narrow-band interference effects. The noise filter output, X, is the input to the forward filter of the DFE. This filter generates a complex sequence, Y, still sampled at RSR by means of an adaptive transversal filter. The compressor strips off the spread-spectrum modulation to produce a bit symbol rate complex sample, C. The detector sums the backward filter output, C, with Z, to form the PSK decision, A. In the absence of decision errors, $\hat{A} = A$. The previous decisions are filtered in the backward filter to produce the complex sample, C. Adaption of the forward and backward filters of the DFE is accomplished during message transmission from an error signal, E, derived in the detector.

DFE SIMULATION AND FIELD TEST RESULTS

To illustrate the performance of the DFE, the time-variant filter in figure 10 was used to simulate an intra-task-force channel. The channel consists of two propagation paths separated by 824 μs—a separation that could occur for a communication range of 426 km (230 nmi). The first path would be the surface wave and the second would be an F-layer reflection from an F-layer height of about 300 km (186.5 statute miles). The two paths have equal loss normalized here to be 0.707. For the first simulation test, the two paths are nonfading. Figure 21 shows the bit error rate versus SNR for signals with spread-spectrum gains of 0, 6, 10, and 16 dB. The SNR is the ratio of bit energy to noise density, where the bit energy includes both the information and reference energies. For the nonfading channel the spread spectrum appears to improve the probability of error performance over nonspread spectrums. Additional tests are required to confirm this, but a possible explanation is that the spread spectrum provides protection against uncanceled intersymbol interference.

A second simulation test was made with a skywave path fading rate, BRMS, of 0.5 Hz. The surface wave was held fixed (no fading). Figure 22 gives the bit error rate results. In this case it appears that with the equalizer, the spread-spectrum modulations are less efficient than the non-spread-spectrum modulation.

Tables 3-5 give parameters characterizing the DFE algorithm. Explanations of these parameters, and of others as well, are given in references 32 and 33. In brief, the ISET numbers are the transversal filter tap delays for the forward filter, expressed in units of the receiver sample interval. Similarly, the JSET numbers are the transversal filter tap delays for the backward filter, expressed in units of the chip symbol interval. Both the forward and backward filters measure their delays relative to their respective inputs. For signals without spread spectrum, the backward filter tap spacing becomes the bit interval.

Table 3 lists the parameters characterizing the DFE algorithm used with each of the spread-spectrum signal simulations. Variations in configuration were required to minimize the error rate for each case.

Table 6 is a summary of field test signals that have been processed with the DFE algorithm. During each time period listed, both a narrow-band (2.4 kHz) and wide-band (96 kHz) signal were transmitted and recorded. The mode, delay, and power are the estimates of the multipath signals based on postsignal processing. Even though the recorded signals

---

[32]Contract report, Decision-Feedback Equalizer Simulation (DFES) – Program Performance Specification, Signatron Inc, Contract N66001-77-C-0248, July 1978.

[33]NOSC TD in preparation, Decision-Feedback Equalizer Simulation (DFES) Documentation Data Base Design, by KL Payne (1981).

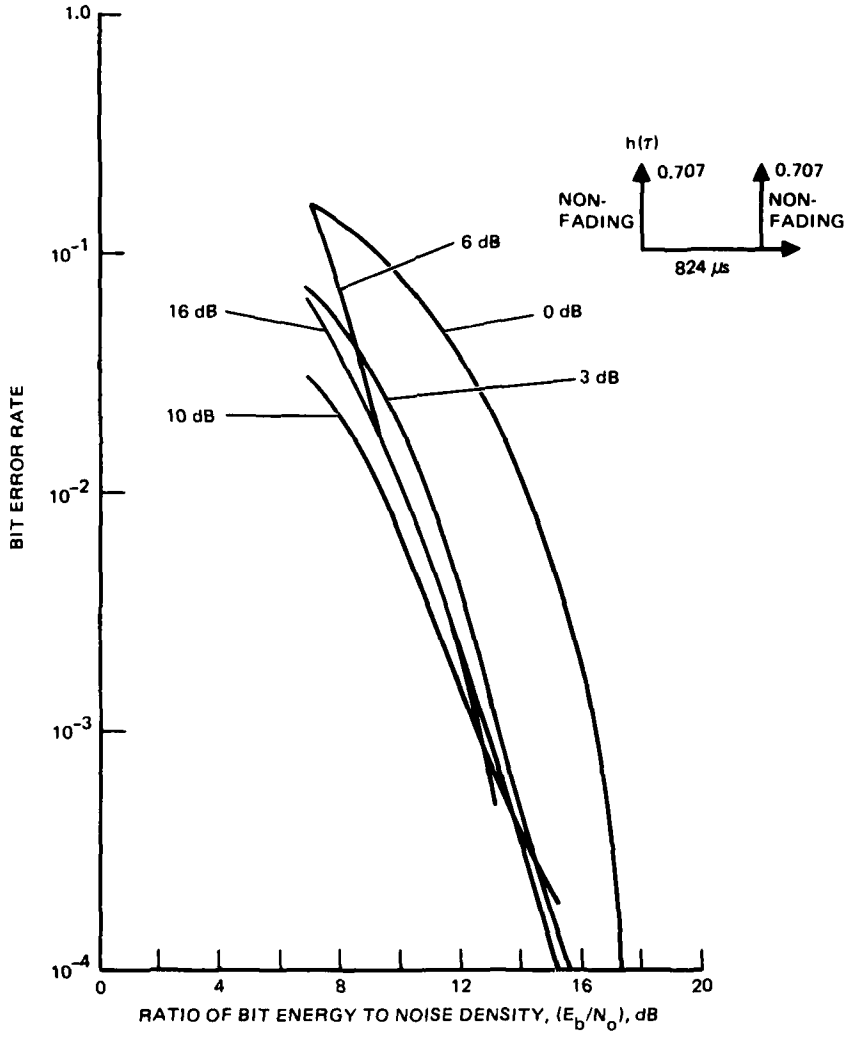

Figure 21. Simulation of bit error rate results for a nonfading channel consisting of surface-wave and skywave paths.

were about 40 s long, the fade rates were not estimated since the fading observed during these time periods was slow. The SNRs in the table are the ratios of signal to atmospheric plus man-made noise recorded during the test. For computer processing, lower SNRs were generated by adding white Gaussian noise to the recorded signals. Tables 4 and 5 give the DFE algorithm parameters used to process the field test signals.

Figure 23 gives the bit error rate versus SNR for narrow-band signals, with the channels dominated by surface-wave propagation. Degradation of SNR is caused probably by the filtering and sampling losses. For the high-SNR portion of the curve, the noise is primarily atmospheric and man-made, thus non-Gaussian.

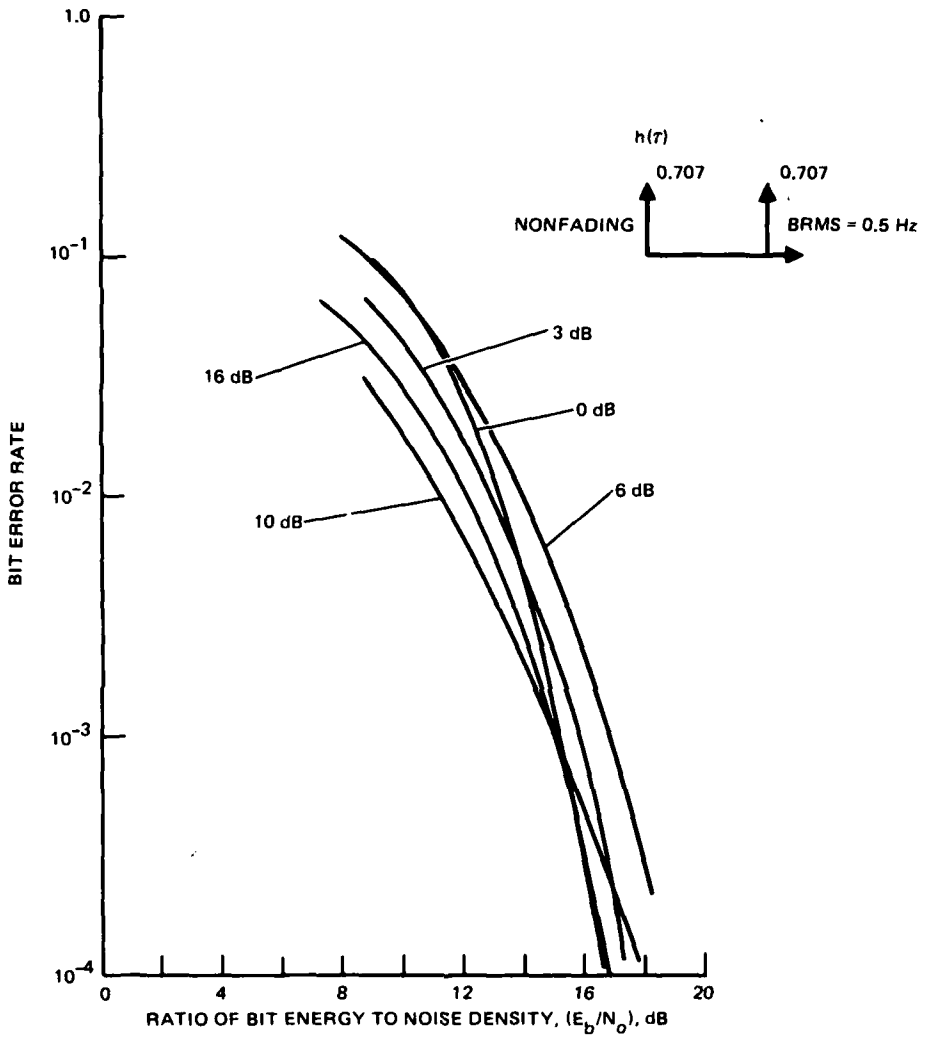

Figure 22. Simulation of bit error rate results for channels consisting of a surface wave and a fading skywave path.

Figure 24 gives the bit error rate versus SNR for narrow-band, prodominantly skywave signals. In each case the skywave signal strength was as strong as or stronger than the surface wave. Tests E and F had little or no fading, so the bit error rate performance was similar to the steady surface-wave results in figure 23. Deep fading during tests G and H caused the bit error rate to fall off much more slowly. The channel in test H consisted of two equal paths separated by 1.4 ms. The channel in test E consisted of a strong E-layer skywave which was undergoing deep fading. The equalizer could do little to improve the error rate in this case.

Figure 25 gives the results for the spread-spectrum modulated signals. The only test was of a 16 dB spread spectrum. Since the spread spectrum could resolve the multipath, the

A – Two-path channel, surface wave and skywave equal and nonfading, separated by 0.824 ms

Spread-Spectrum Gain, dB	Loop Bandwidth, Hz (FF/BF)*	Number of Taps (FF/BF)*	ISET	JSET*	Tap Distribution
0	14/14	8/4	7,6,8,5 1,2,0,3	1,2,4,3	Clustered around delays
3	14/14	8/4	5,4,6,3 1,2,0,7	1,2,3,4	Clustered around delays
6	14/14	10/10	9,8,7,6,5 4,3,2,1,0	1,2,3,4,5 6,7,8,9,10	Dense
10	14/14	8/4	21,20,22,19 1,2,0,3	1,2,20,19	Clustered around delays
16	14/14	8/4	80,79,81,78 1,2,0,3	1,2,79,78	Clustered around delays

B – Two-path channel, surface wave nonfading; skywave delayed by 0.824 ms with Doppler spread of 0.5 Hz

0	15/15	8/4	7,6,5,4 3,2,1,0	1,2,3,4	Dense
3	14/14	8/4	5,4,6,3 1,2,0,7	1,2,4,3	Dense
6	14/14	8/4	4,0,1,2 3,5,6,7	1,3,5,7	Dense
10	14/14	8/4	21,20,22,19	1,2,20,19	Clustered around paths
16	?/?	8/4	80,79,81,78 1,2,0,3	1,2,79,78	Clustered around paths
3	14/14	8/4	5,4,6,3 1,2,0,7	1,2,4,3	Dense

*FF – forward filter
BF – backward filter
ISET – forward-filter tap positions
JSET – backward-filter tap positions

Table 3. DFE configurations for simulations.

ID	Day-Time	Loop Bandwidth (FE/BF)	Number of Taps (FE/BF)	ISET	JSET	Tap Position
A	2 May 1625	--	--	--	--	--
B	6 May 1545	5/1	8/2	8,7,9,6,1,2,0,3	1,2	Dense
C	9 May 1210	5/1	10/4	9,8,7,6,5,4,3,2,1,0	3,4,5,6	Dense
D	13 May 1030	5/1	5/2	2,1,3,0,4	1,2	Dense
E	13 May 1210	5/5	20/6	19 - 0	1 - 6	Dense
F	13 May 1620	5/5	8/4	7,6,5,4,3,2,1,0	1,2,3,4	Dense
G	13 May 1740	5/1	8/2	7,6,5,4,3,2,1,0	1,2	Dense
H	14 May 1605	5/5	20/6	19 - 0	1 - 6	Dense
I	14 May 1720	5/1	8/4	7,6,5,4,3,2,1,0	1,2,3,4	Dense

(See table 3 for an explanation of the abbreviations used in this table.)

Table 4. Narrow-band DFE configurations for field test signals.

ID	Day-Time	Loop Bandwidth (FF/BF)	Number of Taps (FF/BF)	ISET	JSET	Tap Positions
A	2 May 1625	6/6	8/4	0-7	1-4	Dense
B	6 May 1545					
C	9 May 1210	6/6	8/4	0-7	1-4	
D	13 May 1030	6/6	8/4	0-7	1-4	
E	13 May 1210	6/6	8/4	0-7	1-4	Dense
F	13 May 1620	6/6	20/10	0-20	1,3, 5, . . . , 19	Uniform Sparse
G	14 May 1605					
I	14 May 1720					

(See table 3 for an explanation of the abbreviations used in this table.)

Table 5. Wide-band DFE configuration for field test tapes.

ID	Day-Time	Mode*	Delay, ms	Power, dB	Freq, MHz	Rf BW, kHz	Tape (S + N)/N dB	Remarks**
						2.4		
A	2 May 1625	S	0	0	20.124	96		
						2.4	27.9	No fading.
B	6 May 1545	S	0	0		96	23	No fading, no interference.
		S	0	0		2.4	14.6	No fading.
C	9 May 1210	F	1.8	-14	6.835	96	3.3	Strong O-U is 12 dB > sig spec. No fading, est 12-dB SNR w/o O-U.
						2.4	22.1	No fading.
D	13 May 1030	S	0	0	3.357	96	16.3	No interference, no fading.
		S	0	-10		2.4	24.4	Deep fading (15 dB).
E	13 May 1210	E	0.3	0	6.835	96	22.2	Deep fading (8.5 dB).
		S	0	- 5		2.4	17.1	Fading.
F	13 May 1620	E	0.3	0	5.785	96	15.1	No fading.
		F	2.0	-13				
		S	0	-10		2.4	27.3	No fading.
G	13 May 1740	E	0.3	0	5.785	96	18.6	No fading. O-U is 3 dB < sig spec.
		S	0	0		2.4	22.1	Fast fading.
H	14 May 1605	F	1.4	0	6.835	96	11.6	Fast fading. O-U is 3 dB > sig spec.
I	14 May 1720	S	0	0		2.4	20.6	No fading.
						96	1.3	Weak signal, wide-band burst noise.

*S – surface wave
E – E layer
F – F layer

**O-U – other-user interference
sig spec – peak signal spectrum level
est – estimated
w/o – without

Table 6. Summary of field test signals analyzed with the DFE simulator.

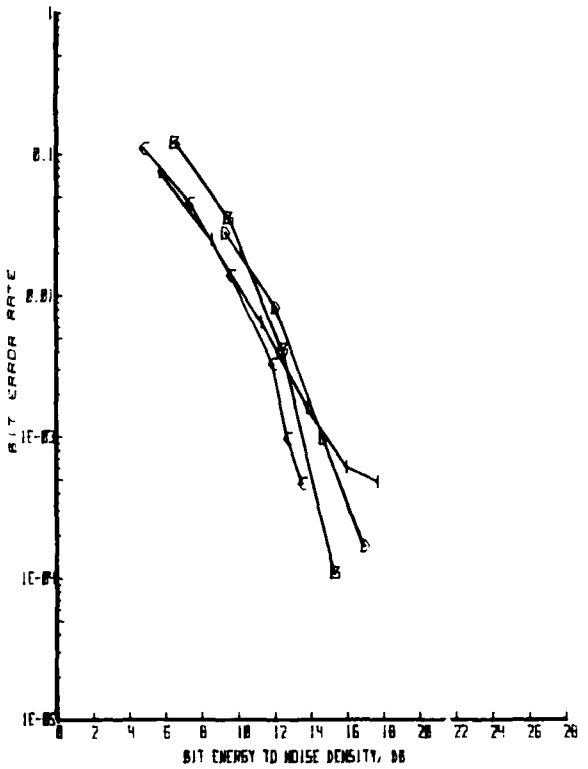

Figure 23. Field test results for narrow-band channels dominated by surface wave. (Plotted from tables 4 and 6)

wide-band equalizer performed better than the narrow-band equalizer in many cases. Also, the wide-band equalizer used a different procedure for positioning the taps, allowing fewer taps to be used than for the narrow-band equalizer. This reduces equalizer self-noise and increases the equalizer ability to track amplitude and phase changes in the received signal.

Specific test data were used to compare th MLSE and DFE algorithms. Figure 26 shows the channel pulse response and SNR for the narrow-band test data recorded 13 May 1980 at 1740. The channel consists of two paths a surface wave and an E-reflection—that are separated by about 300 microseconds. The E-reflection is 10 dB stronger than the surface wave and very stable (nonfading) for the duration of the message. Appendix A gives some additional data on this test transmission.

Figure 27 gives the average bit error rate versus SNR (E_b/N_o) in dB. The results for no intersymbol interference and for parallel-tone DQPSK were derived theoretically. All signaling schemes shown transmit 2400 bits per second. The MLSE without tracking performed poorly probably because of random phase rotations in the received signal. By adding a channel tracking algorithm, the MLSE performance is greatly improved and is close to (within about 2 dB of) the performance achieved on a nonfading channel that has no intersymbol

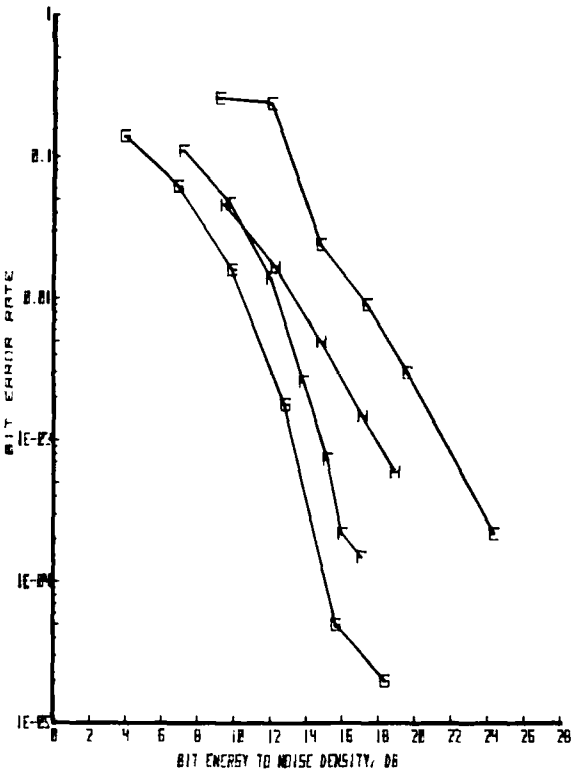

Figure 24. Field test results for narrow-band channels dominated by skywave. (Plotted from tables 4 and 6)

interference. The DFE results are 5 to 6 dB worse than the MLSE and about 2 dB better than the theoretical results for the PT-DQPSK system.

The ranking of the signaling schemes seem to hold for all channels examined, even though the performance curves vary due to different channel multipath conditions. Additional work on processing the remaining field test signals would help provide a more definitive comparison of the signaling schemes.

SUMMARY

The objectives of the Skywave Communication task were to develop communication signal-processing techniques for hf (2-32 MHz) channels that consist of surface-wave and/or skywave modes of propagation. Because of existing interest in the use of spread-spectrum modulation for electronic warfare environments, the task addressed both conventional and spread-spectrum modulation. The approach was (1) to develop a wide-band hf channel model and software simulator, (2) to develop adaptive equalization signal processing techniques and computer simulation software, and (3) to perform an hf field test to record signals for verifying the channel model and signal-processing algorithms.

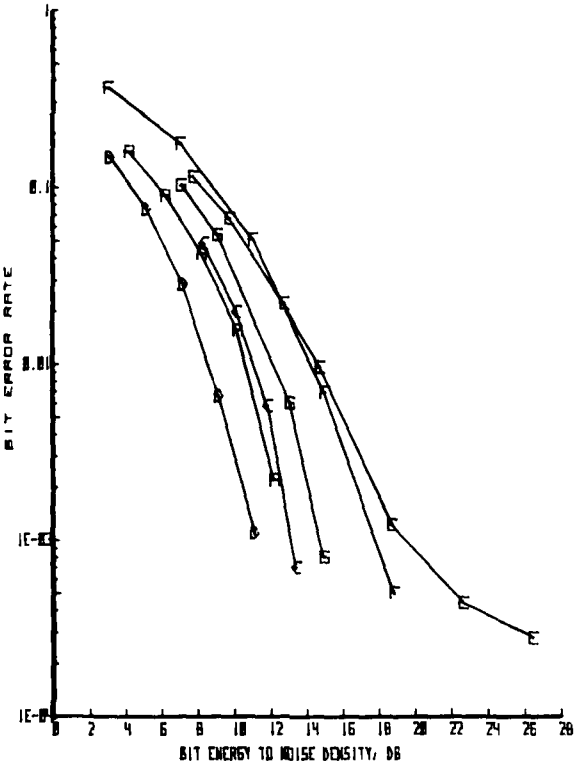

Figure 25. Bit error rate results for 100 kHz spread-spectrum field test signals. (Plotted from tables 5 and 6)

The wide-band hf channel model is based upon a model that was proposed and experimentally verified by CC Watterson et al (ref 8). Their model characterized the hf channel as a time-variant filter whose parameters are stationary random processes. We extended the model to wide bandwidths by taking into account the delay differences between the ordinary and extraordinary wave and the signal distortion caused by variations of phase delay with frequency. It was assumed that the distortion was deterministic and time invariant for the duration of the message. During the Skywave Communication field test of FY80, signals specifically designed to probe the ionosphere channel were transmitted, received, and recorded. Programs subsequently were written to analyze these signals for the purpose of estimating, for the recorded channel conditions, what time duration and bandwidth would provide a good channel model under the above distortion assumption. The next step in this effort would be to interface the program to read the recorded signals and then process the field test data.

Computer simulations were developed for the following signal processing algorithms: RAKE, linear equalization, decision feedback equalization (DFE), and maximum likelihood sequence estimation (MLSE). Simulation tests showed that the MLSE performed the best, followed by the DFE and the linear equalizer. But because the MLSE receiver complexity

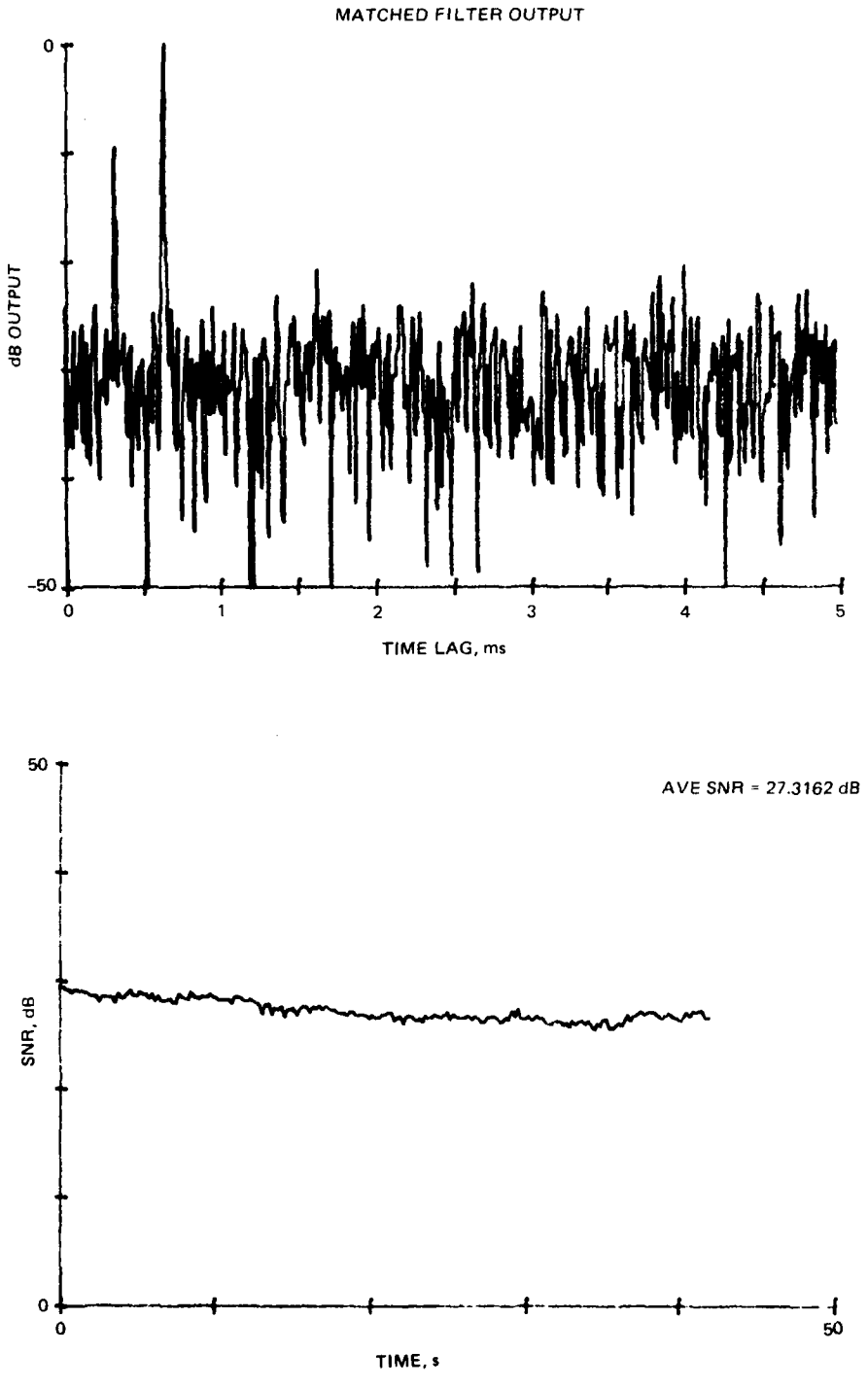

Figure 26. Field test data sample recorded 13 May 1980 at 1740.

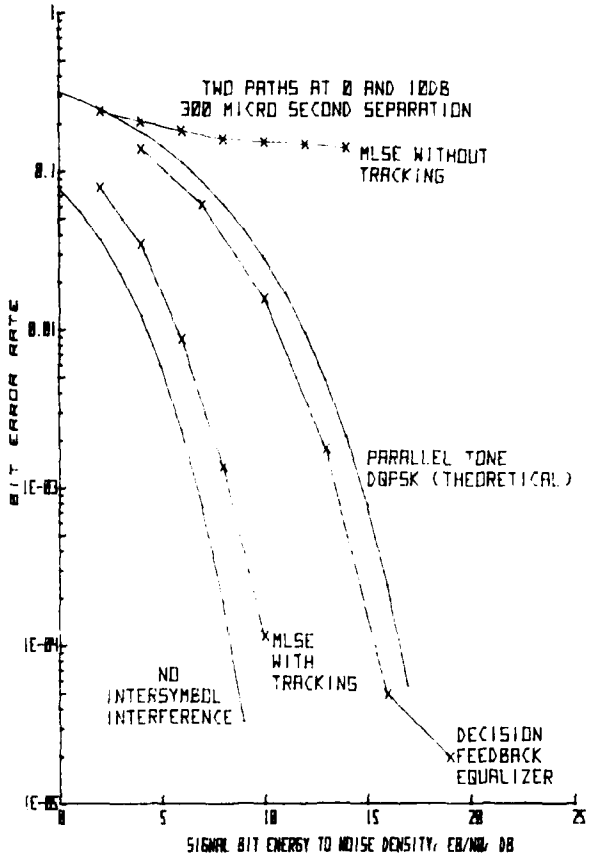

Figure 27. Field test results for Pt Mugu to San Diego channel recorded 13 May 1980 at 1740.

grows exponentially with multipath dispersion whereas the DFE complexity grows only linearly, it was concluded that the DFE was the best choice for the hf channel. The DFE algorithm was extended to incorporate spread-spectrum demodulation. Simulation and field test results are given in this report for 0, 6, 10, and 16 dB spread-spectrum gain.

To illustrate the effect of spread-spectrum gain (SSG) on the required SNR to achieve a given bit error rate performance of the DFE, a two-path channel was simulated that consisted of a surface wave and a skywave. Two sets of runs were made: one with a nonfading skywave and one with the skywave fading at a 0.5 Hz rate. For spread spectrum gains of 0, 3, 6, 10, and 16 dB, the SNRs required to achieve 10^{-3} bit error rate were within 3 dB of each other.

Both narrow-band (3 kHz) and wide-band (100 kHz) signals were transmitted, received, and recorded during the FY80 field tests. A data base was established for the Pt Mugu to San Diego path that included both daytime and nighttime transmissions. (See

appendix A table.) Nine of these signals have been processed with the MLSE and the DFE algorithms. Although the error rate versus SNR curves vary with the channel conditions and algorithms, the ranking of the algorithms seems to be consistent. The MLSE with tracking performs the best, followed closely by the DFE, then by the parallel-tone DQPSK. The disparity between the algorithms is greatest on channels with severe multipath (many paths separated by several milliseconds) and is least on channels with little or no multipath. When the received signal goes into a deep, flat fade (ie a condition in which all paths fade simultaneously), all algorithms perform poorly. A technique such as diversity and/or error-detection-and-correction encoding with interleaving is required to counter deep, flat fades.

In general, the MLSE and DFE provide for significant improvement in bit error rate on channels with severe multipath. The wide-band spread-spectrum signal usually performed better than the narrow-band non-spread-spectrum signal because of the better multipath resolution of the wide band and the spread-spectrum rejection of multipath signals that were undetected by the synchronization algorithm.

The results of the simulated and field test data analyses have demonstrated the application of the adaptive decision feedback equalizer (DFE) to serially modulated signals in the hf band. To achieve best performance for both simulated and field test data, however, the algorithms had to be configured manually for each channel condition. That is, the tapped delay line length, number of taps, tap positions, and LMS step size had to be selected each time a link was to be set up. Further work is required to design a procedure that will automatically configure the equalizer for each channel condition.

RECOMMENDATIONS

A wide-band simulator is a useful tool in evaluating and comparing new signal-processing concepts. The simulator developed by the Skywave Communications task is based upon a wide-band channel model that has not been verified. It is recommended that the data taken during the FY80 field test be processed to verify the wide-band channel model assumptions.

The results of the Skywave Communication task have demonstrated the feasibility of using adaptive equalization on serially modulated transmissions in the hf band. The next step is to embed these algorithms in a real-time data link system and test it over both short-range and long-range paths.

REFERENCES

1. NOSC TD 471 (in preparation), Skywave Communication Techniques: Decision Feedback Equalizer Test Results, by LE Foff and AR King (1981).

2. NOSC TR 208, Addendum 1, Hf Channel Simulator for Wideband Signals, by R Lugannani and HG Booker, 6 November 1978.

3. NOSC TR 208, Hf Channel Simulator for Wideband Signals, by R Lugannani and HG Booker, 31 March 1978.

4. Adaptive Maximum Likelihood Sequence Estimation for the Hf Channel, by LE Hoff and S Norvell; Conference Proceedings for the 13th Asilomar Conference on Circuits, Systems, and Computers, 5-7 November 1979, held at Pacific Grove CA, IEEE Catalog no 79CHiA68-8C, Library of Congress no 79-88185.

5. Interim Technical Report, Hf Channel Adaptive Equalization Algorithm, by P Monsen and S Parl, Signatron Inc, Lexington MA, Contract N66001-77-D-0248, December 1977.

6. Phase 1 Progress Report, Hf Channel Adaptive Equalization Algorithm, by P Monsen, Signatron Inc, Lexington MA, Contract N66001-77-C-2048, 1 February 1978.

7. Report, Decision Feedback Equalizer Simulation (DFES) Data Base Design, by P Monsen, Signatron Inc, Lexington MA, Contract N66001-77-C-0248, July 1978.

8. ESSA Technical Report ERL 122-ITS80, Experimental Verification of an Ionospheric Channel Model, by CC Watterson, JR Juroshek, and WD Bensema, July 1969.

9. National Bureau of Standards Monograph 80, Ionospheric Radio Propagation, by K Davis, 1 April 1965.

10. Radio Wave Propagation and the Ionosphere, 2nd edition, vol I, by YL Alpert, translated by RB Rodman, Consultants Bureau, New York-London, 1973.

11. High Power Radar Studies of the Ionosphere, by JV Evans, Proceedings of the IEEE, vol 63, no 12, p 1636-1650, December 1975.

12. Communication Systems and Techniques, by M Schwartz, W Bennet, and S Stein, p 355, McGraw-Hill, New York, 1966.

13. Evaluation of a Gaussian Hf Channel Model, by HN Shaver, BC Tupper, and JB Lomax, IEEE Transactions on Communication Technology, vol COM-15, no 1, p 79-85, February 1967.

14. Correlation Measurements on an Hf Transmission Link, by F David et al, IEEE Transactions on Communication Technology, vol COM-17, no 2, p 245-256, April 1969.

15. The Impulse Response of a Cold Stratified Plasma in the Presence of Collisions and a Vertical Magnetic Field by a Multiple-Scattering Technique, by KG Gray and SA Bowhill, Radio Science, vol 9, p 559-556, 1974.

16. Transient Response of Stratified Media: Multiple-Scattering Integral and Differential Equations for an Impulsive Incident Plane Wave, by KG Gray and SA Bowhill, Radio Science, vol 9, p 57-62, 1974.

17. Transient Response of Stratified Media: Response to an Arbitrary Incident Plane Wave by KG Gray and SA Bowhill, Radio Science, vol 9, p 63-69, 1974.

18. An Integral Equation for the Transient Response of a Stratified Magnetoplasma, by KG Gray, IEEE Transactions on Antennas and Propagation, vol 24, p 539-541, 1976.

19. Theory of the Electromagnetic Transient Response of the Ionosphere for Plane Wave Excitation, by DA Hill and JR Wait, Pure and Applied Geophysics, vol 90, p 169-186, 1971.

20. Advances in Equalization for Intersymbol Interference, by JG Proakis, paper published in Advances in Communication Theory, edited by Balikrisman and Viterbi, Academic Press, New York, 1975.

21. A Survey of the Communication Theory Literature, 1968-1973, by RW Lucky, IEEE Transactions on Information Theory, vol IT-19, no 5, November 1973.

22. High Speed Modem for Troposcatter, by P Monsen, EASCON, Washington DC, October 1974.

23. Adaptive Equalization of the Slow Fading Channel, by P Monsen, IEEE Transactions on Information Theory, vol COM-22, no 8, August 1974.

24. Theoretical and Measured Performance of a DFE Modem on a Fading Multipath Channel, by P Monsen, IEEE Transactions on Communications, vol COM-25, no 10, October 1977.

25. Communication in Time-Frequency Spread Media Using Adaptive Equalization, by MJ DiTorro, Proceedings of the IEEE, vol 56, no 10, October 1968.

26. NOSC TD 309, Hf Skywave Communications Test Plan, by GP Francis, November 1979.

27. Report CTR-140, Predicted Wave Signalling (Kineplex), by AA Collins and ML Doelz, Collins Radio Co, 20 June 1955.

28. A Communication Technique for Multipath Channels, by R Price and PE Green Jr, Proceedings of the IRE, vol 46, p 555-570, March 1962.

29. Technical Report 258, Error Probabilities for Adaptive Multichannel Reception of Binary Signals, by R Price, MIT Lincoln Laboratory, 23 July 1962.

30. Technical Memorandom 65, An Antimultipath Communication System, by R Price and PE Green Jr, MIT Lincoln Laboratory, 9 November 1956.

31. Adaptive Switching Circuits, by R Widrow and M Hoff Jr, IRE WESCON Conv Rec pt 4, p 96-104, 1960.

32. Contract report, Decision-Feedback Equalizer Simulation (DFES)—Program Performance Specification, Signatron Inc, Contract N66001-77-C-0248, July 1978.

33. NOSC TD in preparation, Decision-Feedback Equalizer Simulation (DFES) Documentation Data Base Design, by KL Payne (1981).

APPENDIX A: FIELD TEST

The purpose of the Skywave Communications Project was to develop and test algorithms to handle intersymbol interference caused by multipath with fading. To aid in this study a channel model was developed. A field test was held in May 1980 between Pt Mugu and Pt Loma (fig A1) to provide real (as opposed to simulated) data for the purpose of testing and validating the signal-processing algorithms and the channel model.

The field test was run in three phases:

1. Back-to-back (19-28 April 1980). The transmit and receive terminals were in the same lab and a coaxial cable was used as a substitute for the hf channel. This phase helped to debug system problems in all but the unused signal transmission portions of the system.

2. Building 33–Model Range (29 April-3 May 1980). The transmitter and receiver separation was about 1.0 km (0.6 mile). This phase was used to continue terminal debugging and testing, with special emphasis on the transmit power amplifier, antenna, and antenna coupler. After the systems were functioning well, baseline data were collected against which to compare the Pt Mugu to Model Range data.

3. Point Mugu–Model Range (6-16 May 1980). This phase produced data with a variety of conditions of multipath (table A1), with one to three paths, and with arrival time differences of up to 8.0 ms.

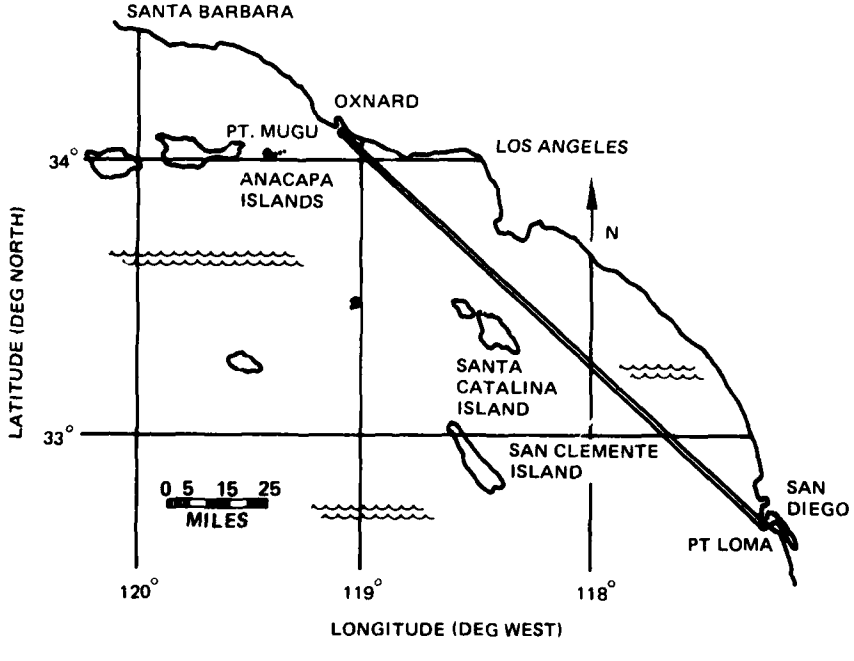

Figure A1. Skywave test path.

Multipath Conditions[1]	Number of Deterministic[2] Signal Transmissions	Number of Short Stochastic[3] Signal Transmissions	Number of Long Stochastic[4] Signal Transmissions	Number of Kineplex Signal Transmissions
S (Pt Mugu-MR)	2	1		
S (Bldg 33-MR)	6	8		
S + E	4	4		
S + F	12	10	2	3
S + E + F	3	3		
S + F + 2F	6	6		
S + Sporadic E			1	

Notes:

(1) Typically E wave was delayed about 0.3 ms, first F wave was delayed about 1.5 ms, and second F wave was delayed about 3.5 ms relative to the surface wave, S.

(2) Deterministic – WB-QPSK, NB-BPSK, comb, cw, sounding.

(3) Short stochastic – sounding signal (0.1172-s pulse duration, 2-s pulse separation, and 100 pulses transmitted) for measuring the channel stochastic parameters.

(4) Long stochastic – sounding signal (0.1172-s pulse duration, 30-s pulse separation, and 100 pulses transmitted) for measuring slow changes of the channel stochastic parameters.

Table A1. Summary of the number of the signal transmissions, Pt Mugu-Model Range (MR).

The field test system is capable of sending and receiving several different signal modulation formats. These modulations can be grouped into two main categories, as follows. (Much of the following on modes was taken from reference A1).

Sounder Modes	Data Modes
cw	Wide-band QPSK
Comb	Narrow-band QPSK
Impulse	Narrow-band BPSK
Short stochastic	Narrow-band BPSK
Long stochastic	Kineplex

A1. NOSC TD 309, Hf Skywave Communications Test Plan, by GP Francis, November 1979.

The sounder mode signals give information on the hf channel parameters. They will be used to verify the channel model. The data modes have the information needed to test signal processing algorithms. A brief description of each mode follows.

The cw signal is centered on the transmitter center frequency. Its purpose is to calibrate the wide-band and narrow-band systems and to measure the received power level.

The comb signal consists of a multitone cw signal (40 tones maximum), each tone separated from the adjacent one by 1.25 kHz. Any combination of channels can be selected by the computer. These data could be used to determine the channel transfer function directly.

The impulse signal consists of a repeating sequence of 1023 bits of a maximal length sequence. Because of its wide bandwidth, high-resolution information on the channel impulse response can be obtained.

The short stochastic and long stochastic data were used to examine changing characteristics of the hf channel. The short stochastic data were used to examine Doppler shift and fading. Its minimum frequency resolution is 0.005 Hz, and the maximum Doppler that can be measured is 0.5 Hz. The long stochastic was designed for examining traveling ionospheric disturbances (TIDs).

The wide-band QPSK signal is a spread-spectrum signal with a baud rate of 2400. Each baud is differently encoded, has one of four possible phases (45°, 135°, 225°, 315°), and is spread out by 40 chips. The resultant chip rate is 96 000 per second. These data will be used to evaluate wide-band signal processing techniques.

The narrow-band BPSK signal is differentially encoded and has a baud rate of 2400; each baud has one of two possible phases (0° or 180°). These data will be used to evaluate a maximum likelihood sequence estimator (MLSE) signal decoder.

The Kineplex signal (narrow-band) consists of 16 tones, like the Link-11 tone package; its baud rate is 2400 and each baud is QPSK modulated. This signal can be used to establish a baseline for comparison between the other narrow-band modulation methods.

SYSTEM OVERVIEW

A description of a typical sampling run follows to show the purpose of the equipment used in the field test.

Before doing anything else, the spectrum analyzer was used to see if our assigned frequencies were in use. If a frequency slot was available, the transmit terminal was phoned and asked to transmit the Loughlin Sounder* signal. The receive terminal then checked the sounder output display, with the receiver connected to a vertical whip antenna and a 45° wire antenna. On the basis of the sounder output, a frequency and an antenna were chosen. Generally the 45° antenna was used for the runs, since it tended to accent the skywave and to suppress other user interference. It was also felt that the 45° antenna was more representative of the shipboard fan antenna. A Polaroid picture was taken of the sounder display to

*Equipment developed by NOSC for measuring hf channel multipath in a 3 kHz bandwidth. See NOSC TN 773, Adaptive Array Hardware Modifications, by PM Hansen and JP Loughlin, 1 October 1979. NOSC technical notes are working documents and do not represent an official policy statement of the Naval Ocean Systems Center, San Diego, California 92152. Further distribution to other than Center employees may be made only with prior approval of Commander, NOSC.

document the conditions just prior to the data collection runs (fig A2). This provided an aid in choosing which data to analyze.

During the run both the transmit and receive terminal were under computer control. Both terminals were synchronized to radio station WWV. This limited absolute time differences to a few milliseconds. This was essential because of the high data rate at which the wide-band data were sampled (192 000 samples per second). With poorly synchronized terminals a large amount of useless noise data would need to have been taken either side of the specified transmission times to ensure that the signal data were collected. This would have created several problems. It would have made it more difficult to find the starting points of signals on magnetic tape, especially with conditions of poor SNR. More magnetic tape would have been required to store useless data. More time would have been required to transfer the data to magnetic tape. As it was, the WB-QPSK and short stochastic data each came close to filling 2400-foot reels of tape. Transferring a typical 5.5-minute combination short stochastic/deterministic run to magnetic tape took about 1.25 hours. Such a run collected about 11×10^6 complex data samples.

Immediately after the run we used the computer to D/A-convert data on the disk for a spot check. We checked to see whether the signals started where they were supposed to start and to get an idea of the SNR. If any problems were found, another run was immediately scheduled and the bad data were discarded. This procedure saved the time and tape that would otherwise be spent on useless data.

During the field test some of the narrow-band and wide-band QPSK tapes were taken back to the lab and run through the channel equalizer algorithms to see whether reasonable error rates were produced, as a check on both the data acquisition system and the equalizer programs.

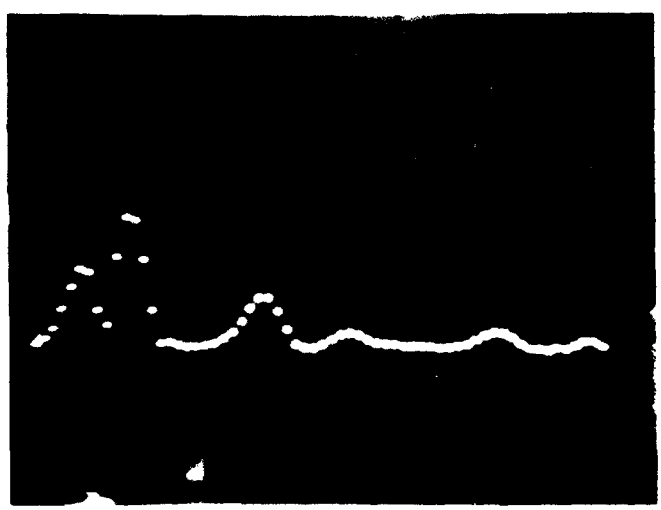

Figure A2. Photo of Loughlin Sounder display taken prior to example in figure 7.

After the field tests, as part of the documentation on each of the channel conditions sampled, plots were made of the following:

The starting points of the received signals.

Power spectra of the noise preceding the wide-band signals and of the signal plus noise.

Matched filter output at the start of the wide-band signals.

TRANSMIT TERMINAL

Figure A3 is a simplified block diagram of the transmit terminal. A PDP-11-03-based computer system was used to control the keyer/modulator that provided all but the Kineplex and Loughlin Sounder modulation. The keyer has an up-converter which fed a Radio Transmitting Set AN/URT-23 power amplifier. The sounder and Kineplex modulator were up-converted by a Radio Transmitter T-827/URT exciter, which then fed the URT-23 power amplifier. The keyer and modulator used a Hewlett-Packard 5065 Rubidium Frequency

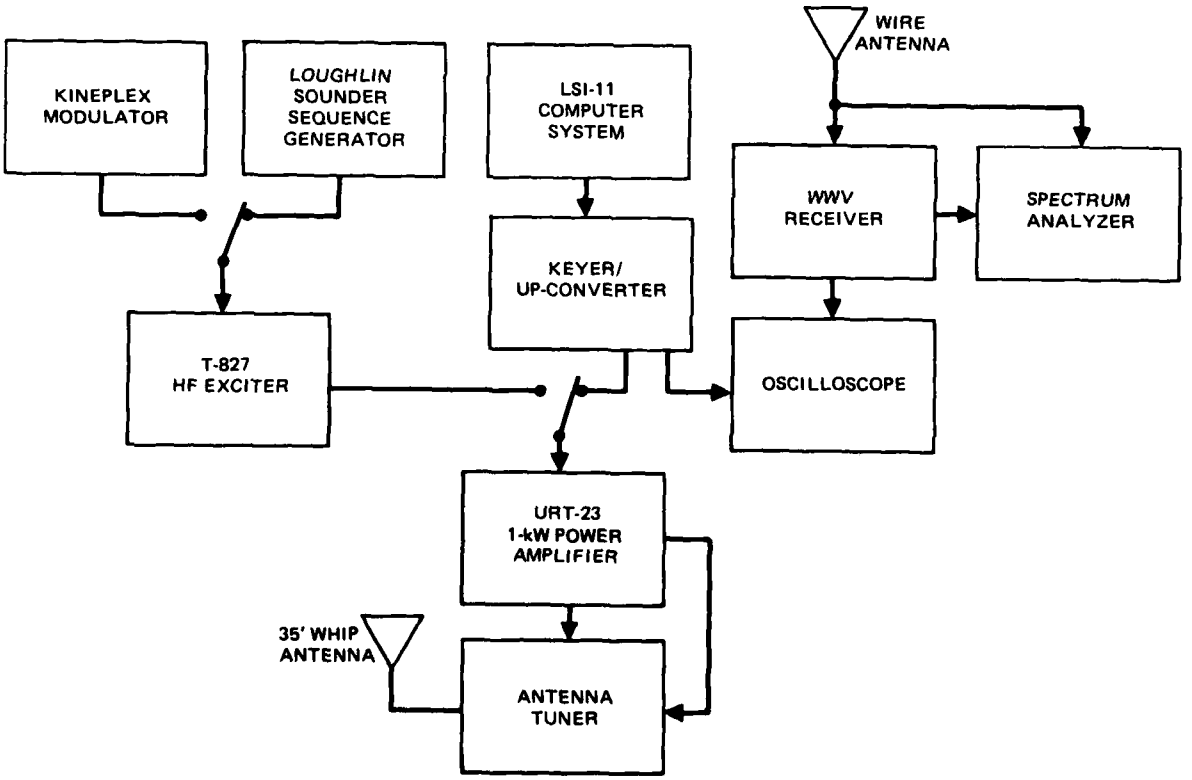

Figure A3. Simplified transmitter terminal block diagram.

Standard with a frequency drift of less than 2×10^{-11} Hz per month. Prior to being moved to Pt Mugu for the field test, this frequency standard was calibrated against a Hewlett-Packard 5061 Cesium Beam Frequency Standard with a specified accuracy of 1×10^{-11} Hz over a 0-50°C range. This was the same standard against which the receiver terminal frequency standard was calibrated daily. A vertical 35-foot whip antenna was used as the transmit antenna. A horizontal wire was used as a receive antenna for the WWV receiver and the spectrum analyzer. The spectrum analyzer was used to monitor the transmitted signal power spectrum and band occupancy.

RECEIVE TERMINAL

Figure A4 is a simplified block diagram of the receiver terminal. A PDP-11/20 computer controlled the receiver data acquisition system. This system digitized the data and temporarily stored it on a Microdata Reflex disk during the transmission.

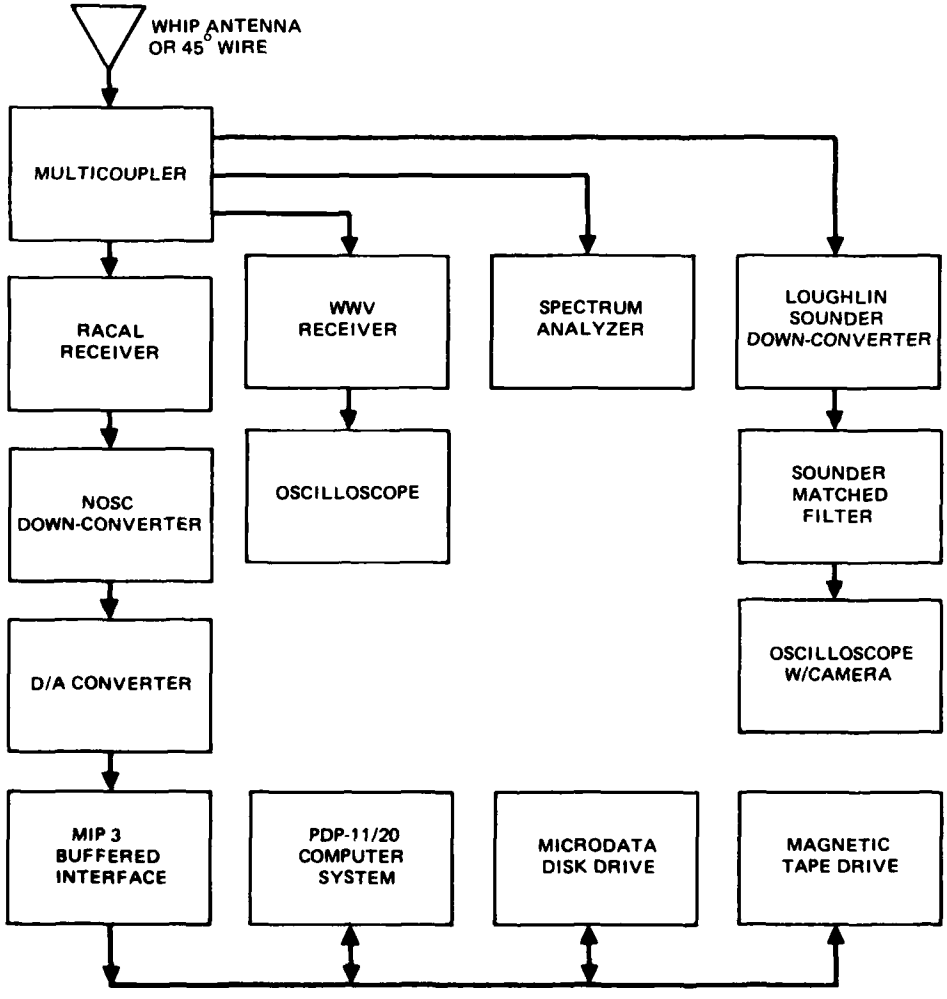

Figure A4. Simplified receiver terminal block diagram.

The Racal receiver, down-converter, and A/D converter were all referenced to a Frequency Electronics FE 1050 Disciplined Time Standard, which is specified as having a frequency drift less than 3.7×10^{-11} Hz per day. This standard was calibrated daily against the same Cesium beam standard as used for calibration of the transmitter terminal's Rubidium standard.

The Loughlin Sounder was used to determine which frequency had the most interesting multipath conditions. The sounder has a time resolution of 300 μs. A spectrum analyzer was used to monitor the received signal strength and to determine whether other user interference was likely to be a problem at a given frequency.

Two antennas were used: a 35-foot vertical whip and a wire at 45° to the horizontal.

RESULTS

There were 33 deterministic runs, 32 short stochastic runs, 3 long stochastic runs, and 3 Kineplex runs (table A1). About half of the short stochastic and deterministic runs were in paired sets, with one immediately following the other. Channels were sampled with one to three paths, and separations between the earliest and latest arriving paths ranged from about 0.3 to 8.0 ms. About 3.6×10^8 complex samples were collected in this field test.

Plots were made of the starting points of all the communications tapes. Figures A5 and A6 show the starting points of a wide-band QPSK signal and a narrow-band QPSK signal, respectively. These figures give a rough feel for the SNR of the data. The SNR is useful for deciding which tape to analyze next and to estimate how well the decoding algorithms should work on the tape. Another useful plot for characterizing wide-band and narrow-band interference on the wideband data tapes is the power spectrum. Examples of the spectrum from the noise blocks and signal blocks of a tape with narrow-band users within the receiver passband are shown in figures A7 and A8 respectively. The passband is 115 kHz for wide-band signals, 1.5 kHz for narrow-band signals. By matched filtering with the Building 33 to Model Range data (only one significant path) as a reference, it was possible to determine the multipath conditions on the channel. A matched filter plot with two significant paths is shown in figure 26 in the main text.

It was difficult to find a frequency at which we could fit our approximately 115 kHz receiver bandwidth without overlapping one or sometimes more narrow-band users. This interference is shown in figure A5 as a high noise level prior to the arrival of the ground wave.

The Loughlin Sounder was useful for real-time characterization of the multipath. Figure A2 is a photo of the sounder display about 10 minutes before the data shown in figure 26. The output of the matched filter is basically the same as the sounder output except that the matched filter output in figure 26 has finer resolution because of the greater bandwidth of the signal.

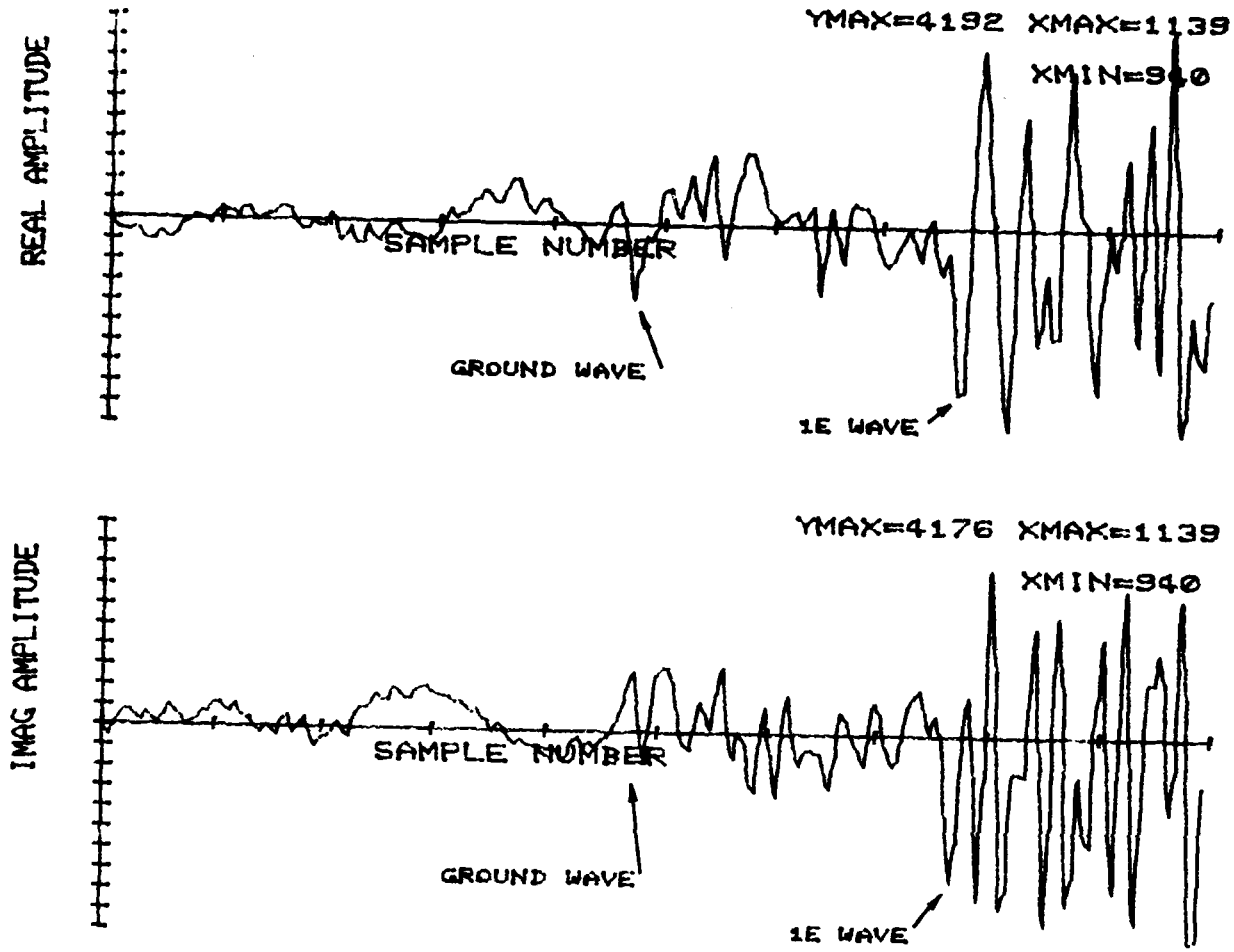

Figure A5. Sample plot of wide-band QPSK data collected, showing (1) noise only on the far left, (2) the arrival of the ground wave, and (3) the later arrival of the 1E wave.

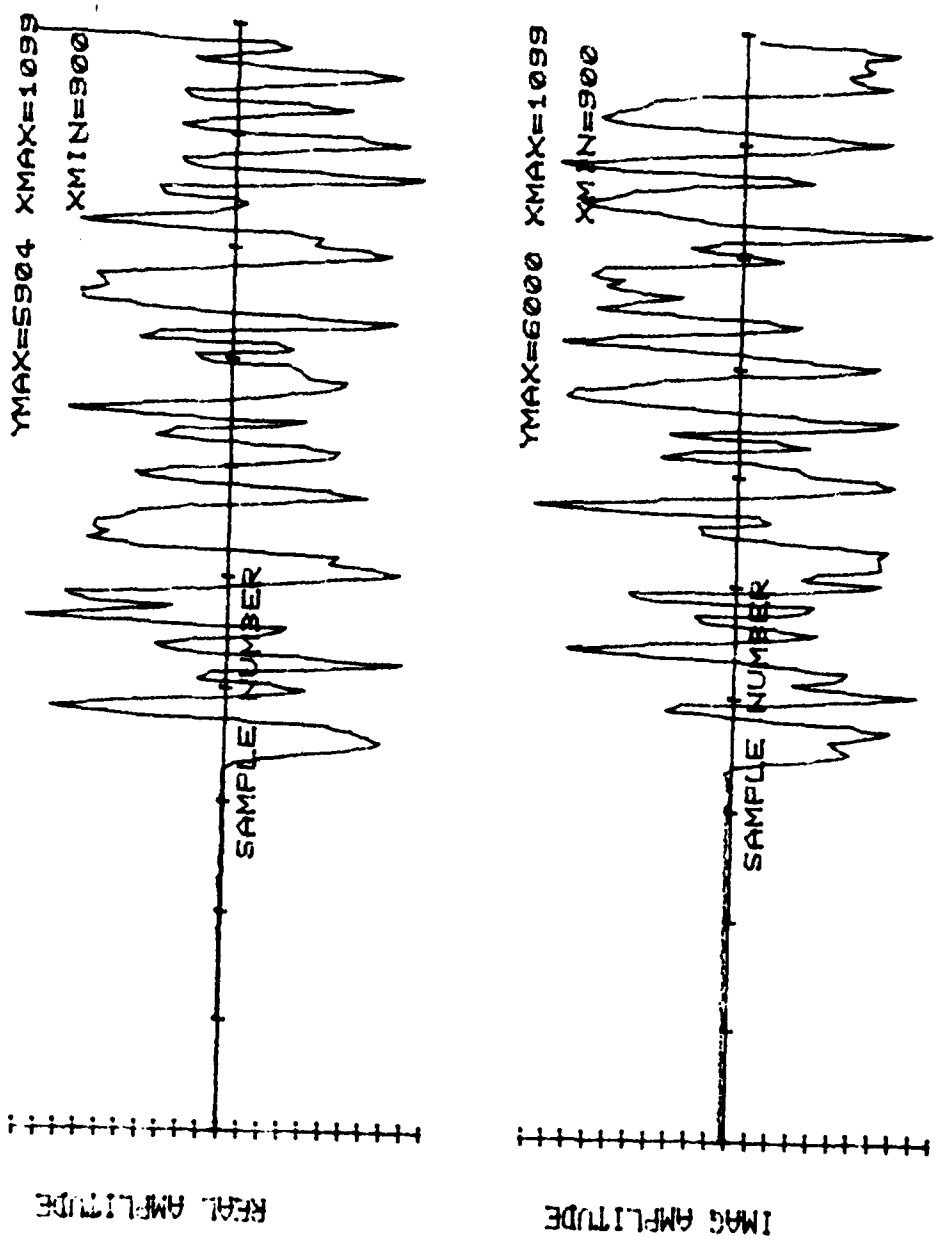

Figure A6. Start point of typical narrow-band data signal.

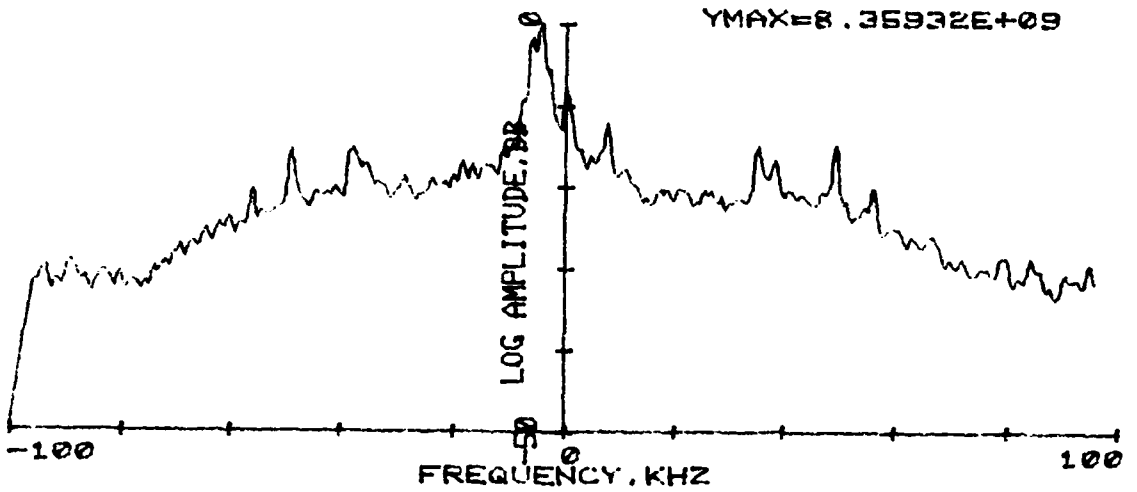

Figure A7. Power spectrum of noise preceding WB-QPSK signal. A number of data were collected 13 May 1980 at 1740 at 5.785 MHz.

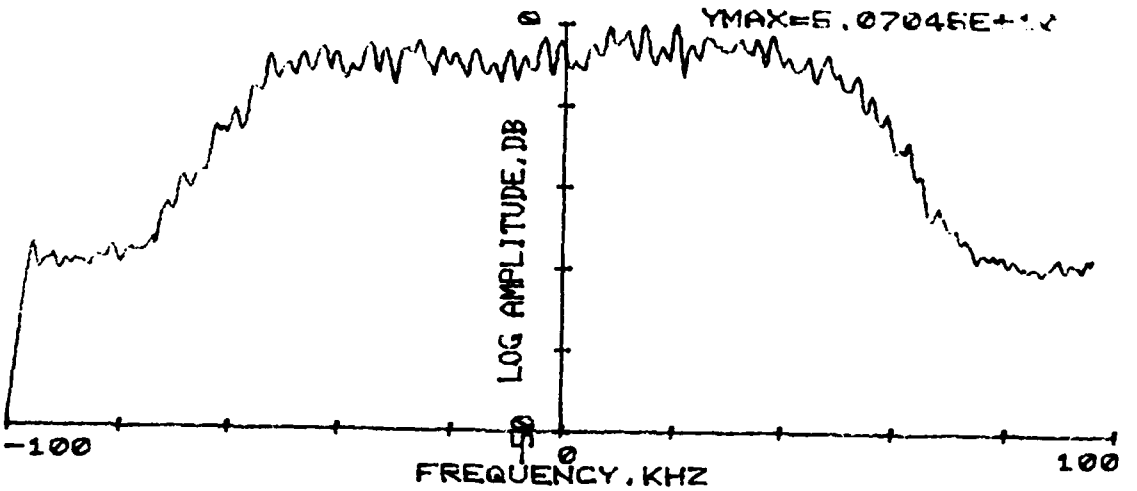

Figure A8. Power spectrum of wide-band QPSK data. Data were collected 13 May 1980 at 1740 at 5.785 MHz.

INITIAL DISTRIBUTION

NAVAL ELECTRONIC SYSTEMS COMMAND
- PME-611A (T. B. HUGHES) (3)
- PME-110-21 (M. PARKER) (3)
- PME-611 (CAPT S. HOLMES) (3)

OFFICE OF NAVAL RESEARCH
- ONR-100 (RADM A. J. BACIOCCIO)

NAVAL RESEARCH LABORATORY
- CODE 7520 (D. I. HIMES)
- CODE 7520 (DR. J. LINNEHAN)

U.S. ARMY COMMUNICATIONS RESEARCH AND DEVELOPMENT COMMAND
FORT MONMOUTH, NJ 07703
- COMMUNICATIONS CENTER
  - ORDCO-COM-RN-3 (MICHAEL DI JULIO)
  - DRDCD-COM-RF-4 (JOHN E. QUIGLEY)
  - DRDCD-COM-RF-4 (DR. T. J. KLEIN)

RADC
GRIFFIS AFB
NEW YORK, NY 13441
- OCCL (DR. JOHN T. GAMBLE)
- DCCT (B. HENDRICKSON)
- DCL (R. A. NORTHRUP)

AIR FORCE AVIONICS LABORATORY
WRIGHT-PATTERSON AFB, OH 45433
- AFAL/AAD (DARLOW BOTHA)
- AFAL/AAD (L. L. GUTMAN)

INSTITUTE FOR TELECOMMUNICATION SCIENCES
- NATIONAL TELECOMMUNICATIONS AND INFORMATION ADMINISTRATION

BOULDER, CO 80303
- CLARK C. WATTERSON

UNIVERSITY OF CALIFORNIA, SAN DIEGO
LA JOLLA, CA 92093
- ELECTRICAL ENGINEERING/COMPUTER SCIENCES DEPARTMENT
  - DR. ROBERT LUGANNANI

TRACOR INC.
9797 AERO DRIVE
SAN DIEGO, CA 92123
- WILLIAM J. FAY

SIGNATRON INC.
12 HARTWELL AVE.
LEXINGTON, MA 02173
- JOHN PEARCE
- DR. PETER MONSEN

RCA
FRONT & COPPER STREETS
CAMDEN, NJ 08102
- PETER REED (MAIL STOPS 10-7-7)

THE MITRE CORPORATION
BEDFORD, MA 01730
- WILLIAM T. BRANDON

DEFENSE TECHNICAL INFORMATION CENTER (12)

END

DATE
FILMED

11-81

DTIC